Hindered Cluster Rotation and ^{45}Sc Hyperfine Splitting Constant in Distonoid Anion Radical Sc$_3$N@C$_{80}{}^-$, and Spatial Spin−Charge Separation as a General Principle for Anions of Endohedral Fullerenes with Metal-Localized Lowest Unoccupied Molecular Orbitals

Alexey A. Popov*,[†,‡] and Lothar Dunsch[‡]

Chemistry Department, Moscow State University, Moscow 119992, Russia, and Group of Electrochemistry and Conducting Polymers, Leibniz-Institute for Solid State and Materials Research Dresden, D-01171 Dresden, Germany

Received June 4, 2008; E-mail: popov@phys.chem.msu.ru

Abstract: DFT calculations of Sc$_3$N@C$_{80}$ in the neutral and anionic states are performed which revealed that in the neutral state of the nitride clusterfullerene the lowest energy structure has C_3 symmetry, while in the anionic and dianionic states the C_{3v} conformer has the lowest energy. Barriers to the cluster rotation inside the cage are also found to increase in the charge states. The ^{45}Sc hyperfine slitting constant, a(Sc), in Sc$_3$N@C$_{80}$ anion radical is calculated by different theoretical approaches and in different conformations of Sc$_3$N cluster. It is found that a(Sc) is strongly dependent on the cluster orientation with respect to the cage, covering a range form −10 to +25 Gauss at the B3LYP/6-311G*//PBE/TZ2P level of theory. A thorough analysis of the computed values as well as comparison of unrestricted and orbital-restricted calculations revealed that the polarization contribution to a(Sc) is about −10 Gauss and does not depend on the cluster orientation. Dependence of the predicted a(Sc) values on the density functional form (LSDA, BP, PBE, BLYP, OLYP, TPSS, B3LYP, and TPSSh), the basis set, as well as on the scalar-relativistic and spin−orbit corrections were investigated. The analysis of the charge distribution in the Sc$_3$N@C$_{80}{}^-$ anion radical revealed an interesting peculiarity of its electronic structure: while the spin density mostly resides on the cluster, only a slight decrease of its charge is found using both Bader and Mulliken definitions of atomic charges. A set of other endohedral metallofullerenes, including nitride clusterfullerenes Sc$_3$N@C$_{2n}$ ($2n$ = 68, 70, 78) and Y$_3$N@C$_{2n}$ ($2n$ = 78−88), carbide clusterfullerenes Sc$_2$C$_2$@C$_{68}$, Sc$_2$C$_2$@C$_{82}$, Sc$_3$C$_2$@C$_{80}$, Ti$_2$C$_2$@C$_{78}$, Y$_2$C$_2$@C$_{82}$, and dimetallofullerenes Sc$_2$@C$_{76}$, Y$_2$@C$_{82}$, La$_2$@C$_{2n}$ ($2n$ = 72, 78, 80), was also studied in the neutral and anionic state, and a spatial charge−spin separation is found to be a general rule for all endohedral fullerenes with high contribution of metal atoms to the LUMO.

Introduction

Among many interesting properties of endohedral fullerenes, the electron transfer from the encaged species to the carbon cage and specific charge states of both the cage and the cluster are of special interest.[1,2] In particular, in nitride clusterfullerenes,[3−5] M$_3$N@C$_{2n}$, a formal six-electron transfer from the cluster to the fullerene can be ascribed,[6,7] albeit the actual value is smaller

due to the back cage-to-cluster donation effect.[8−10] In spite of the formal (−6) charge of the outer carbon cage, M$_3$N@C$_{2n}$ accept electrons relatively easily either in the gas phase[11] or in solution.[12−18] For instance, the gas-phase electron affinity of the archetypical nitride clusterfullerene, Sc$_3$N@C$_{80}$ (2.81 eV),[11] is higher than that of C$_{60}$ (2.666 eV),[19] which is deemed as a

† Moscow State University.
‡ Leibniz-Institute for Solid State and Materials Research.
(1) Shinohara, H. *Rep. Prog. Phys.* **2000**, *63* (6), 843–892.
(2) Akasaka, T.; Nagase, H. *Endofullerenes: A New Family of Carbon Clusters*; Kluwer: Dordrecht, 2002.
(3) Stevenson, S.; Rice, G.; Glass, T.; Harich, K.; Cromer, F.; Jordan, M. R.; Craft, J.; Hadju, E.; Bible, R.; Olmstead, M. M.; Maitra, K.; Fisher, A. J.; Balch, A. L.; Dorn, H. C. *Nature* **1999**, *401* (6748), 55–57.
(4) Dunsch, L.; Yang, S. F. *Phys. Chem. Chem. Phys.* **2007**, *9* (24), 3067–3081.
(5) Dunsch, L.; Yang, S. *Small* **2007**, *3* (8), 1298–1320.
(6) Alvarez, L.; Pichler, T.; Georgi, P.; Schwieger, T.; Peisert, H.; Dunsch, L.; Hu, Z.; Knupfer, M.; Fink, J.; Bressler, P.; Mast, M.; Golden, M. S. *Phys. Rev. B* **2002**, *66* (3), 7.

(7) Kobayashi, K.; Sano, Y.; Nagase, S. *J. Comput. Chem.* **2001**, *22* (13), 1353–1358.
(8) Campanera, J. M.; Bo, C.; Olmstead, M. M.; Balch, A. L.; Poblet, J. M. *J. Phys. Chem. A* **2002**, *106* (51), 12356–12364.
(9) Krause, M.; Popov, A.; Dunsch, L. *ChemPhysChem* **2006**, *7* (8), 1734–1740.
(10) Liu, D.; Hagelberg, F.; Park, S. S. *Chem. Phys.* **2006**, *330* (3), 380–386.
(11) Ioffe, I. N.; Ievlev, A. S.; Boltalina, O. V.; Sidorov, L. N.; Dorn, H. C.; Stevenson, S.; Rice, G. *Int. J. Mass Spectrom.* **2002**, *213* (2–3), 183–189.
(12) Krause, M.; Dunsch, L. *ChemPhysChem* **2004**, *5* (9), 1445–1449.
(13) Krause, M.; Liu, X. J.; Wong, J.; Pichler, T.; Knupfer, M.; Dunsch, L. *J. Phys. Chem. A* **2005**, *109* (32), 7088–7093.
(14) Elliott, B.; Yu, L.; Echegoyen, L. *J. Am. Chem. Soc.* **2005**, *127* (31), 10885–10888.
(15) Cardona, C. M.; Elliott, B.; Echegoyen, L. *J. Am. Chem. Soc.* **2006**, *128* (19), 6480–6485.

good electron acceptor. Up to three reduction steps can be observed for $Sc_3N@C_{80}$ in solution.[12,14,20,21] However, in contrast to C_{60}, which exhibits up to six reversible reductions in some solvents and at lower temperatures,[22] a poor electrochemical reversibility for the electrochemical reduction is observed for $Sc_3N@C_{80}$.[12,14] Moreover, while the electrochemical reversibility of $Sc_3N@C_{80}$ still can be achieved by increasing the scan rates applied and/or lowering the temperature of the experiment[14,21] or varying the solvent,[20] for the clusterfullerenes with larger clusters the electrochemical reversibility cannot be reached up to the scan rates of $70 \ V \cdot s^{-1}$.[15,18] At the same time, it was shown that reduction of $Sc_3N@C_{80}$ and other clusterfullerenes is *chemically* reversible,[14,18,21] and the clusterfullerene can be recovered at the end of a voltammetric cycle; likewise, the stable anion radical can be produced by chemical[23] or electrochemical[14] reduction of $Sc_3N@C_{80}$. These facts indicate that an internal structural reorganization upon the electron transfer can occur for the clusterfullerenes as proposed in ref 18; however, the nature of such a rearrangement remains unclear. Another specific property of the anionic state of $Sc_3N@C_{80}$ is a presumable localization of the spin density on the cluster shown by the large ^{45}Sc hyperfine splitting constant in $Sc_3N@C_{80}^{-}$ anion (55.7 G),[14,23] which agrees well with the localization of the lowest unoccupied molecular orbital (LUMO) in $Sc_3N@C_{80}$ on the cluster predicted by theory.[8,24] However, photoemission and X-ray absorption spectroscopy did not reveal any appreciable changes in the charge state of Sc with potassium doping of $Sc_3N@C_{80}$ up to $K_6-Sc_3N@C_{80}$,[6] which disagrees with the results of EPR spectroscopy and DFT-predicted localization of the LUMO on the cluster. In this article we address the problem of the charge states of $Sc_3N@C_{80}$ theoretically with the use of DFT computations. We show that in the charged states the cluster rotation is significantly hindered, while the lowest energy configuration is different from that in the neutral state. The hyperfine splitting constant of ^{45}Sc in the $Sc_3N@C_{80}^{-}$ radical anion is shown to be extremely sensitive to the position of Sc with respect to the cage carbon atoms and can vary in the range of more than 40 G. Peculiarities of the spin and charge distribution are also discussed, and the spatial spin–charge separation in the anionic state of $Sc_3N@C_{80}$ is discovered and found to be a common property for those endohedral clusterfullerenes which have their LUMO localized on the metal atoms.

Computational Details

Unless otherwise noted, optimization of geometry parameters and Hessian calculations was performed using PBE functional[25]

and TZ2P-quality basis set (full-electron {6,3,2}/(11s,6p,2d) for C and N atoms, and {5,4,4}/(9s,9p,8d) valence part for Sc, Ti, Y, and La) with SBK-type effective core potential for Sc, Ti, Y, and La atoms implemented in the PRIRODA package.[26,27] This basis set will be abbreviated as "TZ2P". The code employed expansion of the electron density in an auxiliary basis set to accelerate evaluation of the Coulombic and exchange-correlation terms.[26] Additional nonrelativistic as well as scalar-relativistic calculations were also performed with PRIRODA using full-electron $\Lambda 11$ ({3,2,1}/(10s,7p,3d) for C, N, and {6,5,3,1}/(19s,15p,11d,5f) for Sc), $\Lambda 22$ ({4,3,2,1}/(12s,8p,4d,2f) for C, N, and {8,7,5,3,1}/ (25s,20p,14d,8f,4 g) for Sc), and $\Lambda 33$ ({5,4,3,2,1}/(14s,10p,5d,4f,3g) for C, N, and {10,9,7,5,3,1}/(27s,22p,16d,10f,8g,4h) for Sc) basis sets from ref 28 (the basis sets used for metal atoms are similar to cc-pwCVDZ, cc-pwCVTZ, and cc-pwCVQZ, respectively). Scalar-relativistic (SR) calculations using Dyall's modified Dirac Hamiltonian[29,30] were performed with PRIRODA and SR-adopted versions of $\Lambda 11$ and $\Lambda 22$ basis sets.

Calculations with hybrid functionals (PBE0, B3LYP, Becke-half-and-half-LYP (BHHLYP hereafter)) were performed with the use of PC GAMESS package[31] and 6-311G* basis set. Some calculations were also performed employing cc-pVTZ, cc-pwCVTZ, and aug-cc-pwCVTZ basis sets for Sc atoms,[32] def-TZVPP for Ti atoms,[33] full-electron TZVPP basis set for Y atoms,[34] and def-TZVPP(-f) basis set with effective core potential[35] for La atoms (note that the f-type polarization function was removed from the original basis set).

Additionally, point energy calculations for $Sc_3N@C_{80}^{-}$ were performed using ORCA[36] to evaluate the values of scalar-relativistic corrections within various modifications of the regular approximation (zeroth-order regular approximation (ZORA),[37] infinite-order regular approximation (IORA),[38] metric-modified IORA[39] (MIORA)). Estimations of the spin–orbit contribution to $a(Sc)$ and g-factor of $Sc_3N@C_{80}^{-}$ anion radical were also evaluated for GGA functionals using the effective potential method (DFT-V_{eff}) implemented in ORCA. In all calculations utilizing GGA density functionals, resolution of the identity procedure was employed.

Bader charges were calculated by numerical grid integration of electronic densities using the Bader code developed in the University of Texas at Austin.[40,41] Accuracy of the charges determined in this work by numeric integration is estimated as $0.01e$. Visualization of molecular orbitals and electronic densities as well as manipulation with PC GAMESS-generated cube files

(16) Chaur, M. N.; Melin, F.; Elliott, B.; Athans, A. J.; Walker, K.; Holloway, B. C.; Echegoyen, L. *J. Am. Chem. Soc.* **2007**, *129* (47), 14826–14829.

(17) Yang, S. F.; Rapta, P.; Dunsch, L. *Chem. Commun.* **2007**, (2), 189–191.

(18) Yang, S. F.; Zalibera, M.; Rapta, P.; Dunsch, L. *Chem. Eur. J.* **2006**, *12* (30), 7848–7855.

(19) Brink, C.; Andersen, L. H.; Hvelplund, P.; Mathur, D.; Voldstad, J. D. *Chem. Phys. Lett.* **1995**, *233* (1–2), 52–56.

(20) Zhang, L.; Chen, N.; Fan, L.; Wang, C.; Yang, S. *J. Electroanal. Chem.* **2007**, *608*, 15–21.

(21) Plonska-Brzezinska, M. E.; Athans, A. J.; Phillips, J. P.; Stevenson, S.; Echegoyen, L. *J. Electroanal. Chem.* **2008**, *614* (1–2), 171–174.

(22) Xie, Q. S.; Perezcordero, E.; Echegoyen, L. *J. Am. Chem. Soc.* **1992**, *114* (10), 3978–3980.

(23) Jakes, P.; Dinse, K. P. *J. Am. Chem. Soc.* **2001**, *123* (36), 8854–8855.

(24) Iiduka, Y.; Ikenaga, O.; Sakuraba, A.; Wakahara, T.; Tsuchiya, T.; Maeda, Y.; Nakahodo, T.; Akasaka, T.; Kako, M.; Mizorogi, N.; Nagase, S. *J. Am. Chem. Soc.* **2005**, *127* (28), 9956–9957.

(25) Perdew, J. P.; Burke, K.; Ernzerhof, M. *Phys. Rev. Lett.* **1996**, *77* (18), 3865–3868.

(26) Laikov, D. N. *Chem. Phys. Lett.* **1997**, *281*, 151–156.

(27) Laikov, D. N.; Ustynyuk, Y. A. *Russ. Chem. Bull., Int. Ed.* **2004**, *54* (3), 820–826.

(28) Laikov, D. N. *Chem. Phys. Lett.* **2005**, *416* (1–3), 116–120.

(29) Dyall, K. G. *J. Chem. Phys.* **1994**, *100* (3), 2118–2127.

(30) Laikov, D. N. In An Implementation of the Scalar Relativistic Density Functional Theory for Molecular Calculations with Gaussian Basis Sets, DFT 2000. Satellite Symposium of the 10th International Congress of Quantum Chemistry, France, 2000; p P43.

(31) Granovsky, A. A. *PC GAMESS, version 7.15*; http://classic-.chem.msu.su/gran/gamess/index.html, 2008.

(32) Balabanov, N. B.; Peterson, K. A. *J. Chem. Phys.* **2005**, *123* (6), 15.

(33) Schäfer, A.; Huber, C.; Ahlrichs, R. *J. Chem. Phys.* **1994**, *100*, 5829–5835.

(34) Ahlrichs, R.; May, K. *Phys. Chem. Chem. Phys.* **2000**, *2*, 943–945.

(35) Dolg, M.; Stoll, H.; Savin, A.; Preuss, H. *Theor. Chim. Acta* **1989**, *75* (3), 173–194.

(36) Neese, F. *ORCA, an ab initio, density functional and semiempirical program package, Version 2.6-35*; Institute for Physical and Theoretical Chemistry: Bonn, 2007.

(37) Chang, C.; Pelissier, M.; Durand, P. *Phys. Scr.* **1986**, *34*, 394–404.

(38) Dyall, K. G.; van Lenthe, E. *J. Chem. Phys.* **1999**, *111* (4), 1366–1372.

(39) Filatov, M. *Chem. Phys. Lett.* **2002**, *365*, 222–231.

(40) Henkelman, G.; Arnaldsson, A.; Jónsson, H. *Comput. Mater. Sci.* **2006**, *36*, 354–360.

(41) Sanville, E.; Kenny, S. D.; Smith, R.; Henkelman, G. *J. Comput. Chem.* **2007**, *28* (5), 899–908.

was done with ChemCraft program.[42] For the sake of clarity, different color codes were used for visualization of the electron density (brown/green), spin density (dark red/dark blue), and molecular orbitals (light blue/light green).

Results and Discussion

The Structure of $Sc_3N@C_{80}$ in the Neutral State. The study of the influence of the charge on the structure of $Sc_3N@C_{80}$ requires that the cluster state in the neutral $Sc_3N@C_{80}$ should be well-known. Surprisingly, in spite of the numerous reports on this subject,[7,8,43,44] the lowest energy configuration of the cluster is still not clear. Nagase and Kobayashi reported the first DFT calculation of $Sc_3N@C_{80}$ with BLYP functional in 2001.[7] They considered two C_s-symmetric conformers with different ways of Sc coordination to the cage, and the structures were found to be isoenergetic within 3.3 kJ/mol. In the same year, Krause at al.[45] reported density functional-tight binding (DF-TB) calculations of the structure and vibrational spectra of $Sc_3N@C_{80}$; the C_3-symmetric conformer was found for $Sc_3N@C_{80}$, but other possible conformers were not reported there. Campanera et al.[8] have reported BLYP computations for several cluster orientations with respect to the cage in $Sc_3N@C_{80}$. The authors have shown that the energy difference between conformers is rather small, and the lowest energy was found for the conformation with C_s symmetry, which was different from the conformers reported by Kobayashi and Nagase;[7] later the same authors reported that the lowest energy configuration has C_3 symmetry (this structure was also different from the C_3-symmetric conformer proposed by Krause et al.).[46,47] Gan and Yuan have also studied several configurations of the cluster inside the cage using local density approximation and BLYP functional.[43] They have found that, at the LDA level, two C_s conformers have the lowest energy; however, single-point BLYP calculations performed with LDA-optimized co-ordinates favored C_{3v}-symmetric conformer, in which all Sc atoms are coordinated to pentagon/hexagon edges. Several other conformers considered by Gan and Yuan had also comparably low relative energies not exceeding 20 kJ/mol.[43] These data show complexity of the problem, which appears due to the shallow potential energy surface for the cluster rotation. Indeed, variable-temperature ^{45}Sc NMR spectroscopy has shown that the cluster is rotating rapidly inside the cage with the approximate barrier of 7 kJ/mol.[48] In such a situation, to get the reliable results from calculations, all symmetry constraints should be lifted while located stationary points are tested by Hessian computations to ensure location of the true energy minimum. As these requirements were not fulfilled in refs 7, 8, and 46, results of those works have to be further verified. Recently, Yanov et al.[44] reported an unconstrained optimization and Hessian computation for several conformers of $Sc_3N@C_{80}$

(42) Zhurko, G. A. *ChemCraft, version 1.5*; http://www.chemcraftprog. com.
(43) Gan, L. H.; Yuan, R. *ChemPhysChem* **2006**, *7* (6), 1306–1310.
(44) Yanov, I.; Kholod, Y.; Simeon, T.; Kaczmarek, A.; Leszczynski, J. *Int. J. Quantum Chem.* **2006**, *106* (14), 2975–2980.
(45) Krause, M.; Kuzmany, H.; Georgi, P.; Dunsch, L.; Vietze, K.; Seifert, G. *J. Chem. Phys.* **2001**, *115* (14), 6596–6605.
(46) Campanera, J. M.; Bo, C.; Poblet, J. M. *J. Org. Chem.* **2006**, *71* (1), 46–54.
(47) Analysis of Cartesian coordinates of C_3 conformer from the ref. 46 revealed that C_s/C_3 conformer from refs. 8 and 46 has acutal C_{3v} symmetry and is the same C_{3v} isomer, which is dicussed in this work.
(48) Wang, X. L.; Zuo, T. M.; Olmstead, M. M.; Duchamp, J. C.; Glass, T. E.; Cromer, F.; Balch, A. L.; Dorn, H. C. *J. Am. Chem. Soc.* **2006**, *128* (27), 8884–8889.

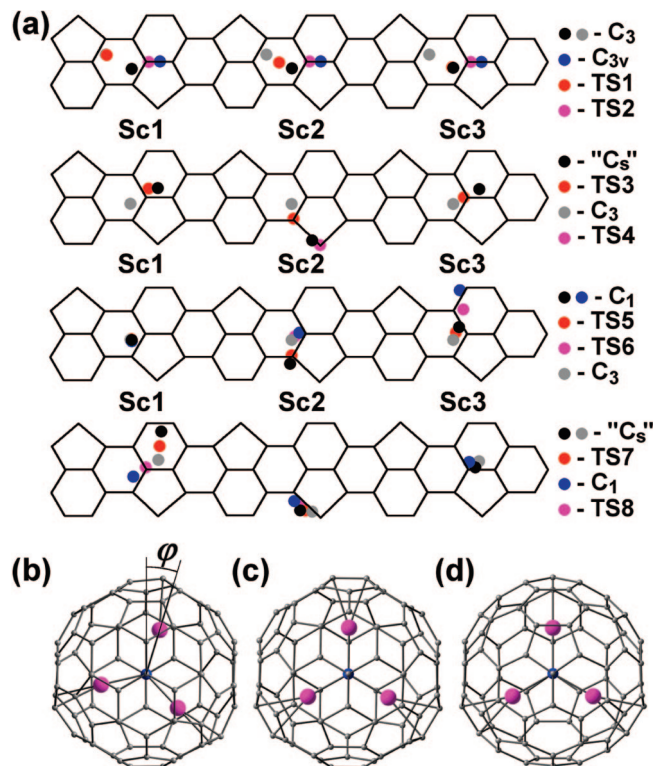**Figure 1.** (a) Schematic drawing of the conformers of $Sc_3N@C_{80}$ computed in this work. Colored dots correspond to the positions at which the arrow radiating from the N atom and passing through the Sc atom crosses the surface of the carbon cage. For the sake of comparison, major conformers are shown several times in different orientations with respect to the shown fragment of the carbon cage. Note that in some cases positions of Sc atoms in different conformers overlap (namely, Sc3 for C_3 and TS1; Sc1 and Sc3 for "C_s" and TS4; Sc1 for C_1, C_3, TS5, and TS6;). (b–d) Molecular structures of C_3 (b), C_{3v} (c), and C_s (d) conformers of $Sc_3N@C_{80}$ optimized at the B3LYP/6-311G* level. Definition of the cluster rotation angle φ is given in (b).

at the HF/STO-3G and B3LYP/STO-3G levels of theory and found several new energy minima. The two lowest energy conformers, with C_s symmetry (the same conformer as found by Gan and Yuan at the LDA level[43]) and with C_3 symmetry (the same as proposed by Krause et al.[45]), were then reoptimized at the B3LYP/6-31G* level, and the lowest energy was assigned to the C_3 conformer, with the C_s-symmetric structure being 2.7 kJ/mol higher in energy. Unfortunately, the use of a very small basis set (STO-3G) for the majority of calculations by Yanov et al.[44] still leaves uncertainty regarding the reliability of their results.

To ensure location of all energy minima that Sc_3N cluster can adopt inside C_{80} cage, we have started geometry optimization of $Sc_3N@C_{80}$ from several conformations reported in the previous works, and each stationary point found in the optimization was further characterized by the Hessian computations. In such a manner, three true energy minima were located (Figure 1, Table 1). The lowest energy configuration has C_3 symmetry, and it is almost the same as reported by Krause et al.[45] and adopted in our previous works.[49–51] In this structure, Sc atoms

(49) Yang, S. F.; Troyanov, S. I.; Popov, A. A.; Krause, M.; Dunsch, L. *J. Am. Chem. Soc.* **2006**, *128* (51), 16733–16739.
(50) Yang, S. F.; Kalbac, M.; Popov, A.; Dunsch, L. *ChemPhysChem* **2006**, *7* (9), 1990–1995.
(51) Popov, A. A.; Dunsch, L. *J. Am. Chem. Soc.* **2007**, *129* (38), 11835–11849.

Table 1. Relative Energies (ΔE, kJ/mol), HOMO−LUMO Gaps (eV), and Frontier Orbital Energies (eV) for Energy Minima and Transition States of $Sc_3N@C_{80}$

		PBE/TZ2P				B3LYP//PBE
conformer	connectivity [a]	ΔE	gap	HOMO	LUMO	ΔE
C_3	−	0.0	1.463	−5.370	−3.907	0.0
C_s	−	4.8	1.310	−5.408	−4.098	1.3
C_1	−	6.5	1.393	−5.380	−3.987	7.1
C_{3v}	−	8.9	1.193	−5.372	−4.179	5.6
D_3	third-order TS	12.9	1.298	−5.361	−4.063	15.3
TS1	C_3, C_3	11.4	1.310	−5.364	−4.054	14.2
TS2	C_{3v}, C_3	9.4	1.293	−5.373	−4.081	6.3
TS3	C_s, C_3	9.0	1.402	−5.390	−3.988	6.2
TS4	C_s, C_s	4.9	1.316	−5.407	−4.091	1.1
TS5	C_1, C_3	6.6	1.414	−5.378	−3.964	7.8
TS6	C_1, C_3	9.0	1.451	−5.397	−3.946	10.4
TS7	C_s, C_s	8.2	1.330	−5.425	−4.095	6.4
TS8	C_1, C_s	9.0	1.371	−5.391	−4.021	5.9

[a] Lists which energy minima are connected by a given transition state.

face hexagons but are displaced from their centers toward the 5/6 edges (conformer in which Sc atoms face the centers of hexagons has D_3-symmetry). The second lowest energy conformer ($\Delta E = 4.84$ kJ/mol) is somewhat distorted from C_s symmetry ("C_s" hereafter), one Sc atom in this structure is facing a 6/6/5 junction, while two others face hexagons close to 5/6 edges (this is the same structure as proposed in refs 43 and 44). Finally, in the higher energy C_{3v} conformer ($\Delta E = 8.91$ kJ/mol) all three Sc atoms are coordinated toward 5/6 edges, and the cluster is slightly pyramidal (the pyramid height $h =$ is 0.073 Å). Note that the C_3 conformer can be obtained from C_{3v} by rotating the cluster by the angle $\varphi = 18.1°$ around the C_3 axis (see Figure 1b for definition of φ), while further rotating to $\varphi = 30°$ results in the D_3 conformer. In accordance with the report by Gan,[43] the D_3-symmetric structure is found to be a third-order transition state.

To find the barriers to the cluster "rotation" inside the cage, we have also located a number of transition states (TSs). For each TS, intrinsic reaction coordinate (IRC) calculations were performed to ensure that a given TS is on the pathway between already known energy minima. This way, we have also found the fourth energy minimum with C_1 symmetry and relative energy of 6.46 kJ/mol (Figure 1a). All TSs located in this works are listed in Table 1 together with the energy minima they connect (see also Figure 1). The highest energy TS (11.40 kJ/mol) corresponds to the rotation of the cluster around the C_3 axis, but it still only slightly exceeds 10 kJ/mol. Thus, our results agree with the previous experimental[3,48] and theoretical[8,43,44] reports on the low energy barriers to the cluster rotation. Significantly, although mathematically C_{3v} and C_1 conformers fulfill all requirements for the energy minima, they cannot be considered as such in the chemical point of view as they are only few tenths of kJ/mol below the energy barriers. For the C_{3v} conformer this can be best illustrated by a section of the potential energy surface along the angle of the cluster rotation around the C_3 axis (Figure 2a; note that C_3 symmetry was fixed in these calculations).

Tables 1 also lists HOMO−LUMO gaps and frontier orbitals energies for all energy minima and transition states located in this work. Significantly, the gaps for the energy minima vary from 1.463 eV for C_3 to 1.193 eV for C_{3v}. In the view of rather small relative energies of the conformers, it can be expected that at room temperatures the fraction of each structure is considerable, thus resulting in rather smeared UV−vis absorp-

tion spectrum of $Sc_3N@C_{80}$ as opposed to $M_3N@C_{80}$ with larger metals (Y and lanthanides), for which larger rotation barrier and relative energies of conformers are predicted[43] (see Figure S1 in Supporting Information for comparison of the UV−vis absorption spectra of $Sc_3N@C_{80}$ and $Y_3N@C_{80}$).

Our calculations on $M_3N@C_{80}$ with larger clusters (M = Y, Lu) have shown that with the increase of the cluster size the C_3 energy minimum is approaching closer to the D_3 transition state (i.e., rotation angles are 19.0° for Lu and 22.2° for Y as opposed to 18.1° for Sc and 30° for D_3 symmetry); this trend was also revealed by X-ray single crystal studies.[52,53] To explore this peculiarity in more detail, we have also computed the sections of the potential energy surface for $Y_3N@C_{80}$ (deemed as large cluster) and $Lu_3N@C_{80}$ (the cluster size is intermediate between Sc_3N and Y_3N). In Figure 2a these curves are given in comparison to that of Sc. Both the $Y_3N@C_{80}$ and $Lu_3N@C_{80}$ are characterized by the drastic increase of the rotation barrier at C_{3v} geometry (in fact, Lu_3N and Y_3N clusters become significantly pyramidal in the C_{3v} state, with the nitrogen displacement out of the M_3 plane of 0.359 and 0.470 Å, respectively) and a decrease of the rotation barrier at D_3 configuration (note that Gan and Yuan reported that D_3-symmetric structure had the lowest energy in the calculations of $Y_3N@C_{80}$ conformers;[43] however, they did not consider the C_3 conformer). These data show that the actual minimum configuration is a result of the subtle balance between the cluster size and the cluster location at the preferable coordination sites. It should be noted that the coordination to the metal increases pyramidalization of the carbon atoms, and pyramidalization of pyrene-type carbon atoms (triple-hexagon junctions) is known to be less energetically favorable than that of carbon atoms on pentagon/hexagon/hexagon junctions (PHHJs). As a result, the metal tends to be coordinated to PHHJs (for instance, pentagon/hexagon edge as in C_3 conformer). However, this coordination type appears to be impossible for the larger clusters due to the limited inner space of the cage, and the large metals shift to the center of the hexagon (closer to D_3 conformer) as this conformation allows longer M−N and M−C distances. Such a dependence of the preferable cluster orientation on its size also implies that, if different theoretical approaches tend to predict different M−N bond lengths for the same clusterfullerene, the relative energies and structures of the conformers can vary from method to method and from basis to basis. To check how our results for $Sc_3N@C_{80}$ can be affected by the choice of a different theoretical approach, we have also performed point energy calculations at the B3LYP/6-311G* level for all minima and transition states found at the PBE/TZ2P level (this combination of functionals and basis sets will be further denoted as B3LYP// PBE). B3LYP//PBE calculations did not result in qualitative changes in the conclusions; however, some variation in the relative energies can be seen (Table 1). For instance, the relative energies of the "C_s" and C_{3v} conformers with respect to the C_3 conformer are reduced, while the energy of D_3 and TS1 transition states are increased at the B3LYP level. Besides, B3LYP//PBE calculations indicate that the "C_s" conformer should probably have a rigorous C_s symmetry, as TS4 is predicted to have a lower energy than the "C_s" conformer. For the C_3, C_s, C_{3v} and D_3 structures we have also performed full

(52) Stevenson, S.; Chancellor, C.; M., L. H.; Olmstead, M. H.; Balch, A. L. *Inorg. Chem.* **2008**, *47* (5), 1420–1427.
(53) Zuo, T.; Olmstead, M. M.; Beavers, C. M.; Balch, A. L.; Wang, G.; Yee, G. T.; Shu, C.; Xu, L.; Elliott, B.; Echegoyen, L.; Duchamp, J. C.; Dorn, H. C. *Inorg. Chem.* **2008**, *47* (12), 5234–5244.
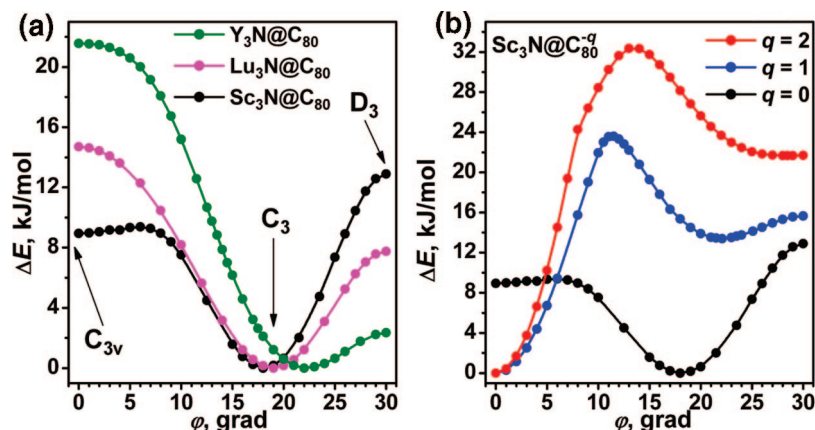
Figure 2. Section of the potential energy surface along the cluster rotation angle φ computed at the PBE/TZ2P level for: (a) $Sc_3N@C_{80}$, $Lu_3N@C_{80}$, and $Y_3N@C_{80}$; (b) for $Sc_3N@C_{80}$, $Sc_3N@C_{80}^-$, and $Sc_3N@C_{80}^{2-}$.

Table 2. Relative Energies (ΔE, kJ/mol), Adiabatic Electron Affinities (E_A, eV), Sc−N ($d(Sc-N)$, Å) and Sc−C ($d(Sc-C)$, Å) Bond Lengths, Atomic and Cluster Charges, and $a(Sc)$ hfc (gauss) in B3LYP/6-311G*-Optimized Conformers of $Sc_3N@C_{80}$ in Different Charge States (q)

	C_{3v}			C_s		$C_3{}^a$	D_3	
	$q=0$	$q=-1$	$q=-2$	$q=0$	$q=-1$	$q=0$	$q=0$	$q=-1$
ΔE(B3LYP//PBE)	5.6	0.0	−	1.3	4.7	0.0	15.3	26.1
ΔE(B3LYP/6-311G*)	5.5	0.0	−	0.7	3.8	0.0	15.9	27.1
E_A, eV[b]	2.660	0.365	−	2.572	−	2.323	2.488	−
$d(Sc-N)$, Å	2.015	1.995	1.991	2.015, 2.021 (x2)	1.979, 2.012 (x2)	2.018	2.019	2.016
$d(Sc-C)$, Å	2.271	2.287	2.297	2.240, 2.269 (x2)	2.248, 2.300 (x2)	2.259	2.372	2.375
$q(Sc)$, Bader	1.76	1.71	1.69	1.73, 1.77 (x2)	1.74, 1.70 (x2)	1.77	1.78	1.75
$q(Sc_3N)$, Bader	3.52	3.36	3.28	3.50	3.36	3.53	3.57	3.49
$q(Sc)$, Mulliken	1.38	1.33	1.31	1.38, 1.38 (x2)	1.39, 1.31 (x2)	1.38	1.40	1.39
$q(Sc_3N)$, Mulliken	2.88	2.75	2.69	2.89	2.78	2.88	2.96	2.92
spin population on Sc_3N	−	0.64	−	−	0.62	−	−	0.40
$a(Sc$, B3LYP//PBE)	−	28.53	−	−	8.34, 26.26, 30.09	−	−	−6.18
$a(Sc$, B3LYP/6-311G*)	−	35.69	−	−	14.44, 34.06 (x2)	−	−	−4.29

a B3LYP/6-311G* optimization of C_3 conformer of $Sc_3N@C_{80}^-$ resulted in D_3-$Sc_3N@C_{80}^-$. *b* Adiabatic electron affinity is calculated as the energy difference between optimized $Sc_3N@C_{80}^-$ and $Sc_3N@C_{80}$. For the C_3 conformer, the energy of D_3-$Sc_3N@C_{80}^-$ was used for the anionic state.

geometry optimization at the B3LYP/6-311G* level (in these calculations molecular symmetry was used, but Hessian computations could not be done due to high computational demands). In accord with point energy calculations, full optimization has shown that C_3 is still the lowest energy conformer followed by C_s ($\Delta E = 0.70$ kJ/mol) (Table 2). As B3LYP/6-311G* predicts by ~0.01 Å shorter Sc−N bond lengths than PBE/TZ2P, the relative energy of the D_3 isomer at the B3LYP/6-311G* level is further increased ($\Delta E = 15.93$ kJ/mol), lower energy is predicted for C_{3v} isomer ($\Delta E = 5.48$ kJ/mol), while Sc atoms in the C_3 isomer are found to be closer to the pentagon/hexagon edge with a φ value of 17.2° (as compared to 18.1° in PBE/TZ2P-optimized structure; the structure in which N, Sc, and two Sc-coordinated carbon atoms are coplanar would have $\varphi = 11.6°$).

Structure and Energetics of $Sc_3N@C_{80}$ in the Charged States. As the lowest energy conformers of $Sc_3N@C_{80}$ in the neutral state have been located, we proceeded to computations of the anionic states of $Sc_3N@C_{80}$. Optimization of the mono- and dianions at the PBE/TZ2P level was performed starting from all energy minima listed in Table 1 and also from the D_3 conformer. For the closed-shell dianions, Hessians were calculated to confirm the location of the energy minima. Finally, calculations of the section of the potential energy surface along the angle of the cluster rotation around the C_3 axis were also performed similar to the neutral state (Figure 2b).

The calculations have shown that charging of the $Sc_3N@C_{80}$ results in considerable variations of the relative energies of the conformers. The energy difference between C_3 and D_3 conformers is reduced to infinitesimal values of 2.24 and 0.02 kJ/mol for the mono- and dianion. Besides, at the PBE/TZ2P level the D_3 conformer is only the first-order transition state as opposed to the neutrally charged $Sc_3N@C_{80}$, while the potential energy surface in the vicinity of C_3 and D_3 conformers is very shallow. However, C_3 is not the lowest energy conformer any more. The C_{3v} conformer is found to be a ground state of $Sc_3N@C_{80}$ in −1 and −2 charged states being by 13.44 and 21.67 kJ/mol more stable than C_3, respectively. The second most stable conformer besides C_{3v} is C_s ($\Delta E = 2.30$ and 3.27 kJ/mol in mono- and dianion, respectively), while the relative energy of the C_1 conformer is significantly increased with charging ($\Delta E = 13.31$ and 18.84 kJ/mol in the mono- and dianion, respectively). These changes are also reflected in the section of the potential energy surface shown in Figure 2b. It can be seen that a deep minimum is developed for C_{3v}, while the C_3 configuration is getting closer to the D_3 state. Importantly, the barrier to the cluster rotation is significantly increased (to ~25 kJ/mol for mono- and 32 kJ/mol for dianion).

Geometry parameters of the cluster and their variation with φ are also affected by the charge of the clusterfullerene. In particular, while for the neutral $Sc_3N@C_{80}$ the Sc−N bond lengths are increasing from 2.030 Å for C_{3v} to 2.036 Å for D_3
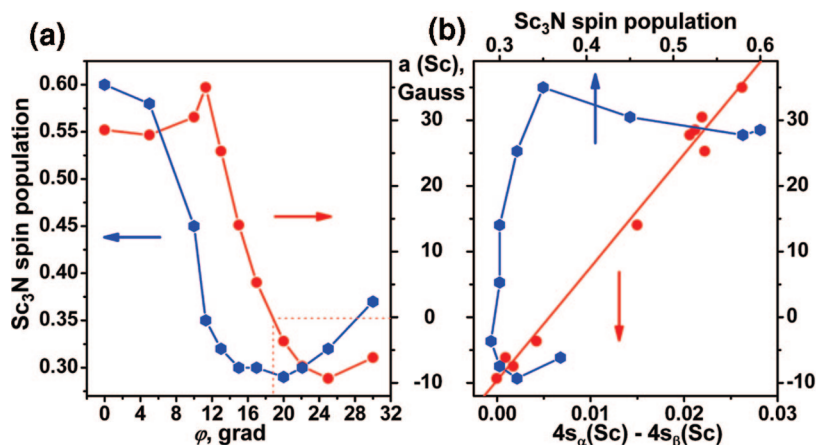
Figure 3. (a) $a(Sc)$ hfc (red) and net spin population on Sc_3N cluster (blue) in $Sc_3N@C_{80}^-$ as a function of the cluster rotation angle φ; (b) $a(Sc)$ hfc in $Sc_3N@C_{80}^-$ as a function of the net spin population on the Sc_3N cluster (blue) and on the $4s(Sc)$ polarization (red). Straight line for the latter is the result of the least-squares fitting ($a(Sc, G) = -9.64 \pm 1.10 + (1724 \pm 66) \cdot \Delta 4s_{\alpha-\beta}(Sc)$; $R^2 = 0.989$). The values used in the graphics were computed at the B3LYP/6-311G*//PBE/TZ2P level.

conformers, a larger spread of values, from 2.014 to 2.037 Å, is found for the anion (see Figure S2 (Supporting Information) for more details).

To verify these findings, we have also performed B3LYP//PBE point energy calculations for selected points of Figure 2b and for C_{3v}, D_3, C_3, C_s, and C_1 conformers. A full optimization of C_{3v}, D_3, C_3, and C_s conformers at the B3LYP/6-311G* level was also performed for the monoanions. B3LYP calculations showed qualitatively the same results in terms of the preferable stability of the conformers (Table 2); however, the barriers are predicted to be even lager (up to 31 kJ/mol for the monoanion) than those found at the PBE/TZ2P level (see Table S1 [Supporting Information]). Note also that at the B3LYP/6-311G* level the C_3-$Sc_3N@C_{80}^-$ anion merges into the D_3-$Sc_3N@C_{80}^-$. Table 2 also lists adiabatic electron affinities (E_A) calculated for these conformers. Significant variation of E_A's (up to 0.2–0.3 eV) is found. Therefore, the 0/− reduction potential of $Sc_3N@C_{80}$ noticeably depends on the conformer participating in redox process. Specifically, it may result in a significant shift between reduction and reoxidation potentials found experimentally[12,14,18] because different conformers are the ground states for respective charge forms.

In summary, DFT calculations show that in the anionic states of $Sc_3N@C_{80}$ the ground state is changed from C_3 to C_{3v}, while the cluster rotation becomes significantly hindered. Interestingly, chemical modification of $Sc_3N@C_{80}$ via exohedral addition also results in the increase of the cluster rotation barriers.[54,55]

Sc Hyperfine Constant in $Sc_3N@C_{80}^-$. General Discussion.
By locating the lowest energy conformers of $Sc_3N@C_{80}^-$, the analysis of the ^{45}Sc hyperfine splitting constant ($a(Sc)$ hfc) in $Sc_3N@C_{80}$ can be done. First, we analyze the results of B3LYP//PBE calculations in view of the large number of different conformers computed at this level. Table 2 lists the $a(Sc)$ hfc values for different energy minima, while Figure 3 shows the dependence of the $a(Sc)$ on the cluster rotation angle covering the range from the D_3 to the C_{3v} conformers (see Table S1

[Supporting Information] for the full set of $a(Sc)$ hfc values at different φ). Analysis of the data in Table 2 and Figure 3 clearly demonstrates that $a(Sc)$ hfc dramatically depends on the cluster orientation inside the cage. In particular, $a(Sc)$ varies from -6 G for D_3 to 25 G for C_{3v}, changing the sign at an angle of $\sim18.5°$. The largest value at the B3LYP//PBE level, 32 G, is obtained for a configuration in which the cluster is deviated from C_{3v} by 11.3° (this state also corresponds to the point with the largest relative energy, 32.0 kJ/mol, in Figure 2b). For the "C_s" conformer the average hfc of two quasi-symmetric Sc atoms is also quite large, 28.2 G, while the hfc of the third Sc atom is only 8 G.

Analysis of the localization of the single-occupied molecular orbitals (SOMO) in $Sc_3N@C_{80}$ and the spin density distribution as well as the spin population showed that in all conformers the cluster contribution to SOMO and the spin density is at least significant and in some cases dominant (the net spin population on the cluster varies from 0.3 to 0.7). The shape of the Sc-anchored lobes of SOMO and spin density varies from pure d_{z^2}-orbital oriented parallel to the C−C bond in C_{3v} conformer to the complex-shaped distribution with the lobes oriented toward the closest C atoms, as in D_3 conformer (Figure 4). The correlation between the spin population and $a(Sc)$ is rather poor, indicating the complex nature of $a(Sc)$ (Figure 3b). This fact emphasizes that $a(Sc)$ is determined by the value of the spin density in a definitive point (at the nuclei), while the spin population is an integral value. These two quantities do not necessary correlate. Therefore, care should be taken when the experimental hfc is used to make the conclusions about the spin density distribution in the monoanion radical. The large spin population at the cluster does not necessarily lead to the large hfc, as can be exemplified by the configuration of $Sc_3N@C_{80}^-$ in which the cluster is rotated by $\varphi = 18.5°$ from C_{3v}. While the net spin population of the cluster in this structure is ~0.35, $a(Sc)$ is essentially zero. This becomes obvious when the fact is considered that d orbitals have nodes on the nuclei, and thus their participation in SOMO does not directly affect $a(Sc)$. The latter is determined only by the spin polarization of s shells, either valence (4s for Sc) or core (1s−3s), to which d orbitals can contribute indirectly through the spin polarization. NBO analysis revealed that the occupation of 4s states of Sc in all configurations of the cluster within $Sc_3N@C_{80}^-$ is very small

(54) Wakahara, T.; Iiduka, Y.; Ikenaga, O.; Nakahodo, T.; Sakuraba, A.; Tsuchiya, T.; Maeda, Y.; Kako, M.; Akasaka, T.; Yoza, K.; Horn, E.; Mizorogi, N.; Nagase, S. *J. Am. Chem. Soc.* **2006**, *128* (30), 9919–9925.

(55) Shustova, N. B.; Popov, A. A.; Mackey, M. A.; Coumbe, C. E.; Phillips, J. P.; Stevenson, S.; Strauss, S. H.; Boltalina, O. V. *J. Am. Chem. Soc.* **2007**, *129* (38), 11676–11677.
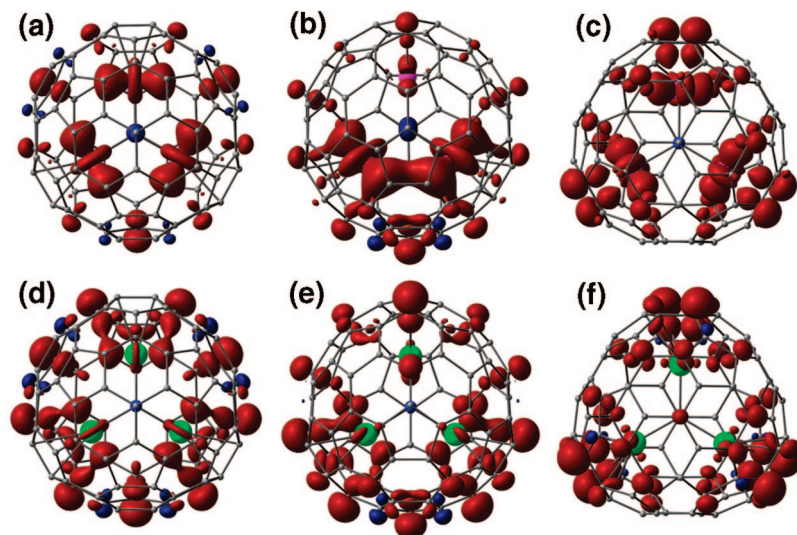
Figure 4. Spatial distribution of spin density in conformers of $Sc_3N@C_{80}^-$ (C_{3v}-a, C_s-b, D_3-c) and $Y_3N@C_{80}^-$ (C_{3v}-d, C_s-e, D_3-f) plotted with isodensity value of 0.0016 au, dark red denotes regions with positive spin density, dark blue denotes regions with negative spin density. Calculations were performed at the B3LYP/6-311G* level for $Sc_3N@C_{80}^-$, and at the B3LYP/TZVPP//PBE/TZ2P level for $Y_3N@C_{80}^-$.

(~0.05), i.e. the spin population on Sc atoms is largely ascribed to 3d orbitals. However, despite the very small contribution of the 4s shell, its spin polarization (defined as the difference of 4s-α and 4s-β populations) shows a perfect linear correlation with a(Sc) hfc ($R^2 = 0.989$), indicating the dominance of 4s shell in determining a(Sc) value in $Sc_3N@C_{80}^-$. With this respect we should note that usually two major terms in the hfc are to be distinguished.[56,57] The direct term arises from the s-orbital contribution to SOMO and is always positive. The polarization term arises from the spin polarization of core s shells by SOMO and can be either positive or negative. In these terms, the polarization of 4s is affecting the direct term, and hence one can conclude that the variation of the direct term is responsible for the large change of a(Sc) with the cluster orientation. However, the intercept in the correlation between 4s polarization and a(Sc) is −9.6 ± 1.1 G, and this value can be readily ascribed to the polarization term. Interestingly, the polarization term appears to be independent of the cluster orientation. When the 4s polarization vanishes, the polarization term is dominating (e.g., in the C_3 conformer). These results agree with the benchmarking calculations of Munzarová et al.[58,59] which have shown that (i) the polarization term in 3d-block transition metals is always negative and that (ii) the polarization term for a given metal is weakly dependent on the bonding situation (just as observed in this work for Sc).

The influence of the polarization term can be also revealed by a comparison of the results obtained in unrestricted (U) and restricted (RO) calculations, as the polarization term appears only in unrestricted calculations and vanishes for the RO calculations. This situation will be discussed below.

(56) Gerson, F.; Huber, W. *Electron Spin Resonance Spectroscopy of Organic Radicals*; WILEY-VCH Verlag GmbH & Co. KGaA: Weinheim, 2003.
(57) Kaupp, M.; Buhl, M.; Malkin, V. G. *Calculation of NMR and EPR Parameters. Theory and Applications*; WILEY-VCH Verlag GmbH & Co. KGaA: Weinheim, 2004.
(58) Munzarová, M. L.; Kubáček, P.; Kaupp, M. *J. Am. Chem. Soc.* **2000**, *122* (48), 11900−11913.
(59) Munzarová, M. DFT Calculations of EPR Hyperfine Coupling Tensors. In *Calculation of NMR and EPR Parameters. Theory and Applications*; Kaupp, M., Buhl, M., Malkin, V. G., Eds.; Wiley-VCH Verlag GmbH & Co. KGaA: Weinheim, 2004; pp 463−472.

^{45}Sc Hyperfine Constant in $Sc_3N@C_{80}^-$. Method and Basis Set Dependence. When comparing the results of calculations to the experimental data, the fact has to be taken into account that the experimentally observed a(Sc) hfc is an effective value, resulting from the averaging of all Sc_3N positions in the multiple available minima. The statistical weight for each conformer is determined by the Boltzmann distribution, and the relative energies of the C_3 and C_1 conformers demonstrate that their contribution should be negligible, while the C_{3v} conformer is expected to be dominant. The C_s conformer is also quite stable and can thus compete with the C_{3v} conformer. The precise ratio of the C_s and C_{3v} conformers is difficult to estimate because of the small difference of their relative energies (Table 2) and the unknown reliability of DFT in the prediction of these quantities (there is a lack of experimental information on the relative energies of the conformers that would allow verification of the accuracy of theoretical approach). However, the C_s conformer is asymmetric (see Tables 2, 3 for DFT-predicted with a(Sc) hfc), and significant contribution of this structure would result in either (i) deviations of the ESR spectrum from that obtained for three equivalent Sc atoms or (ii) the smaller effective a(Sc) value, if the cluster rotation is sufficiently fast. While the experimental ESR spectrum is undoubtedly corresponding to three equivalent Sc atoms[14,23] and hence the symmetry-reducing contribution of C_s conformer can be neglected, the second possibility cannot be excluded, i.e. that experimentally observed a(Sc) is smaller than it would be for the C_{3v} conformer alone. We assume that the experimental ESR spectrum of $Sc_3N@C_{80}^-$ can be modeled by only the spectrum of C_{3v} conformer, and thus results of the calculations are at an upper bound for theoretically predicted a(Sc) in $Sc_3N@C_{80}^-$.

Theory predicts that the C_{3v} conformer has the largest a(Sc) hfc value, but even for this conformer either B3LYP//PBE or B3LYP/6-311G* predicts a(Sc) hfc (28.5 or 35.7 G, respectively) which is too low as compared to the experimental value of 55.7 G.[14,23] Hence, a series of additional calculations of a(Sc) hfc in C_{3v}-$Sc_3N@C_{80}^-$ were performed to reveal the method and basis set dependence of DFT-predicted a(Sc). $Sc_3N@C_{80}^-$ is still too large to be studied by a full complexity of theoretical methods such as CCSD(T) that are known to provide very

Table 3. DFT-Computed a(Sc) in $Sc_3N@C_{80}^-$ (in G)[a]

method [b]	method/coords [c]	a(Sc)	method	method/coords	a(Sc)
PBE/Λ11	PBE/Λ11	31.35	B3LYP/6-311G*	B3LYP/6-311G*	35.69
SRD-PBE/Λ11	SRD-PBE/Λ11	40.88	RO-B3LYP/6-311G*	B3LYP/6-311G*	43.86
PBE/Λ22	PBE/Λ22	23.71	B3LYP/cc-pVTZ(-g) [d]	B3LYP/6-311G*	40.08
SRD-PBE/Λ22	PBE/Λ22	29.59	RO-B3LYP/cc-pVTZ(-g)[d]	B3LYP/6-311G*	42.43
PBE/Λ33	PBE/Λ33	25.08	B3LYP/cc-pwCVTZ[d]	B3LYP/6-311G*	36.96
mPBE/Λ33	mPBE/Λ33	24.15	RO-B3LYP/cc-pwCVTZ[d]	B3LYP/6-311G*	42.64
BLYP/Λ33	BLYP/Λ33	27.79	B3LYP/aug-cc-pwCVTZ[d]	B3LYP/6-311G*	37.89
OLYP/Λ33	OLYP/Λ33	13.29			
			B3LYP/6-311G*	B3LYP/6-311G*,C_s	14.44, 34.06 (x2)
PBE/6-311G*	PBE/TZ2P	20.95	RO-B3LYP/6-311G*	B3LYP/6-311G*,C_s	15.96, 45.60 (x2)
RO-PBE/6-311G*	PBE/TZ2P	30.34	B3LYP/cc-pwCVTZ[d]	B3LYP/6-311G*,C_s	14.29,36.39 (x2)
PBE0/6-311G*	PBE/TZ2P	25.63			
B3LYP/6-311G*	PBE/TZ2P	28.53	B3LYP/6-311G*	B3LYP/6-311G*,D_3	−4.29
BHHLYP/6-311G*	PBE/TZ2P	31.06	RO-B3LYP/6-311G*	B3LYP/6-311G*,D_3	7.17

[a] Unless otherwise noted, the values given are for C_{3v} conformer. [b] "method" column denotes the level at which a(Sc) was computed. [c] "method/coords" denotes the level at which coordinates were optimized. [d] The basis set used for Sc atoms is given, while the 6-311G* basis set was used for C and N atoms.

accurate estimations of the hfc in transition metals,[57] and hence this study is limited to DFT only. However, even within DFT, there are several factors influencing predicted values:

(a) the type of exchange-correlation functional. Predicted a(Sc) can be sensitive to the exact form of exchange and /or correlation functionals, as well as to the fraction of the exact exchange included (from zero for GGA functionals such as PBE, to 20% as for B3LYP to 50% for BHHLYP functional).[58−60] In general, hybrid functionals are known to be more accurate than generalized gradient approximation (GGA) functionals; however, they are more computationally demanding. In particular, the density-fitting technique considerably accelerates calculations with GGA functionals, but appears to be nonefficient for hybrid functionals;

(b) the basis set used can considerably affect predicted values. For instance, a good description of the core-valence interactions is required if the polarization term has an important contribution to the a(Sc);

(c) the relativistic correction may be important;

(d) the data described above show that structural parameters (e.g., Sc−N bond length) are also important.

Unfortunately, evaluation of all of these effects in one concise study is hardly possible, largely because the extensive computations with hybrid functional exceed our computational abilities. At the same time, such calculations are indeed possible for GGA functionals. Therefore, we performed a series of calculations focusing on each of the mentioned factors.

First, we have studied the basis set dependence of a(Sc) predicted by PBE functional. The study included a gradual increase of the basis set from Λ11 to Λ22 to Λ33, and a full optimization of the structure was performed with each basis set. Computed a(Sc) hfcs are listed in Table 3. The largest a(Sc), 31.35 G, is predicted when a relatively small Λ11 basis set is used, while the increase of the basis set results in the drop of the a(Sc) values to 23.71 (Λ22) and 25.08 G (Λ33). These changes are accompanied by the increase of the Sc−N bond length from 2.008 (Λ11) to 2.015 (Λ22) to 2.016 (Λ33) and a shortening of the Sc−C bond from 2.288 (Λ11) to 2.281 (Λ22) to 2.280 (Λ33). At the same time, the Sc-coordinated C−C bond does not depend on the basis set, retaining the length of 1.472 A. One can conclude that these values are almost converged for the triple-ζ Λ22 basis set and further increase of the basis

does not result in significant changes. However, there is a significant difference between Λ11 and Λ22 basis sets. Though PBE/Λ11 shows a better agreement with experimental a(Sc) hfc, this should be ascribed to the fortuitous cancelation of errors. In particular, a small basis set shortens optimized Sc−N bond lengths, and a(Sc) is significantly dependent on their lengths, the shorter distance resulting in larger hfc.

In the framework of GGA-PBE functional, the effect of the Dyall's scalar-relativistic (SRD) corrections was also studied. While values for Sc−N, Sc−C, and C−C bonds optimized at SRD-PBE/Λ11 level are virtually identical to PBE/Λ11 values, the a(Sc) value is increased by 9.5 G when SR corrections are taken into account. SRD-PBE/Λ22//PBE/Λ22 calculation also revealed that the SR corrections increase a(Sc) hfc by 5.9 G.

Munzarová et al.[58,59] have shown that for the radicals with transition metals in which SOMO has mainly a d-character with a small admixture of 4s, the metal hfc is mostly dependent on the form of exchange functional, while the correlation functional is relatively unimportant. In this respect, we have tested a modified version of the PBE functional[61] (mPBE) and BLYP[62,63] and OLYP[63,64] GGA functionals, all with the Λ33 basis set and a full optimization of the anion (see Table 3). It was found that the mPBE/Λ33-predicted a(Sc) hfc is virtually identical to its PBE/Λ33 counterpart. The BLYP/Λ33 value is slightly larger (27.8 G); however, OLYP/Λ33 predicts much smaller a(Sc), 13.3 G. Thus, aside from Handy−Cohen-optimized exchange functional (O), which substantially reduces the predicted a(Sc) hfc, all other methods do not result in a significant variation of a(Sc) (note that the correlation PBE functional is similar to other correlation functionals provided by Perdew and co-workers, including PW91[65] and P86[66]).

The method-dependence of the a(Sc) was also studied for several hybrid functionals. In view of much higher computational demands, only single-point calculations with a 6-311G* basis set were performed using PBE/TZ2P-optimized coordinates. Calculations were performed with PBE0, B3LYP, and BHHLYP functionals (the latter uses a half an d-half-combination of the Becke exchange functional and the exact exchange)

(60) Kossmann, S.; Kirchner, B.; Neese, F. *Mol. Phys.* **2007**, *105* (15−16), 2049−2071.

(61) Adamo, C.; Barone, V. *J. Chem. Phys.* **2002**, *116* (14), 5933−5940.
(62) Becke, A. D. *Phys. Rev. A* **1988**, *38* (6), 3098−3100.
(63) Lee, C.; Yang, W.; Parr, R. G. *Phys. Rev. B* **1988**, *37* (2), 785−789.
(64) Handy, N. C.; Cohen, A. J. *Mol. Phys.* **2001**, *99* (5), 403−412.
(65) Perdew, J. P. PW91. In *Electronic Structure of Solids '91*; Ziesche, P., Eschrig, H., Eds.; Akademie Verlag: Berlin, 1991; p 11.
(66) Perdew, J. P. *Phys. Rev. B* **1986**, *33* (12), 8822−8824.

Table 4. $a(Sc)$ in $Sc_3N@C_{80}^-$ (in gauss) Computed Using Nonrelativistic (NR) and Scalar-Relativistic Approximations (ZORA, IORA, MIORA); Spin−Orbit Correction to $a(Sc)$, and g- Factors[a]

method[b]	method/coords[c]	$a(NR)$	$\Delta a(ZORA)$[d]	$\Delta a(IORA)$[d]	$\Delta a(MIORA)$[d]	$\Delta a(SO)$[d]	g-factor
LSDA (SVWN5)	PBE/TZ2P	33.54	0.34	2.58	1.22	−0.22	2.0000
LSDA (SVWN5)	B3LYP/6-311G*	40.04	0.51	2.91	1.42	−0.24	1.9997
LSDA (PW)	B3LYP/6-311G*	40.08					
BP	PBE/TZ2P	28.31	0.81	2.46	1.53	−0.26	1.9994
BP	B3LYP/6-311G*	34.09	1.17	3.65	1.98	−0.27	1.9990
PBE	PBE/TZ2P	25.66	1.28	2.60	2.06	−0.23	1.9997
PBE	B3LYP/6-311G*	31.80	0.98	2.51	1.62	−0.25	1.9993
revPBE	B3LYP/6-311G*	29.54					
mPBE	B3LYP/6-311G*	28.72					
BLYP	PBE/TZ2P	26.35	1.92	1.74	2.14	−0.26	1.9988
BLYP	B3LYP/6-311G*	31.98	0.83	1.71	1.48	−0.27	1.9983
OLYP	PBE/TZ2P	17.92	1.04	1.23	1.11	−0.29	1.9993
OLYP	B3LYP/6-311G*	22.28	1.00	1.61	1.34	−0.31	1.9988
TPSS	PBE/TZ2P	26.33	1.39	4.87	2.02	−0.24	1.9996
TPSS	B3LYP/6-311G*	32.40	1.50	5.52	2.14	−0.25	1.9992
B3LYP	B3LYP/6-311G*	37.30	0.66	2.13			
TPSSh	B3LYP/6-311G*	34.91	1.63	5.41			

[a] The values are computed using ORCA package for C_{3v} conformer; [b] "method" column denotes the functional used in calculations of $a(Sc)$, the basis set was always set cc-pwCVTZ for Sc and 6-311G* for C and N atoms; [c] "method/coords" denotes the level at which coordinates were optimized; [d] $\Delta a(ZORA)$ is defined as the difference $a(ZORA) - a(NR)$; an analogous definition is used for IORA, MIORA, and spin−orbit (SO) corrections.

as well as PBE/6-311G*, the latter was included to compare to the $a(Sc)$ values predicted by hybrid functionals. The values obtained with all of these methods show that the use of a hybrid functional results in a somewhat larger $a(Sc)$ hfc, the smallest value predicted by PBE (20.95 G), followed by PBE0 (25.63 G), B3LYP (28.53 G), and BHHLYP (31.06 G).

The influence of geometry parameters can be envisaged by comparing the results of the full optimization at the B3LYP/6-311G* level to the result of the B3LYP//PBE single point calculation (Table 2). The full optimization results in a significant increase of $a(Sc)$ as compared to the PBE/TZ2P geometry in line with the shorter Sc−N bond predicted by B3LYP (we have already noted that shorter Sc−N bonds lead to larger $a(Sc)$ hfc). Thus, in the further study of the basis set dependence of $a(Sc)$ within the hybrid functional, B3LYP/6-311G*-optimized coordinates were used, and the Sc basis set was varied while retaining the 6-311G* basis set for C and N. B3LYP/cc-pVTZ(-g)//B3LYP/6-311G* calculations revealed a further increase of $a(Sc)$ up to 40.08 G; however, the split of the core basis within cc-pwCVTZ basis set resulted in a decrease of $a(Sc)$ back to 36.96 G. Finally, when the cc-pwCVTZ basis set was augmented with diffuse functions, this resulted in a slight increase of the $a(Sc)$ value up to 37.89 G. The B3LYP/aug-cc-pwCVTZ//6-311G* value is the most refined one obtained in this work within nonrelativistic DFT. Based on SRD-PBE calculations discussed above, a further increase of $a(Sc)$ can be expected in relativistic theory making it closer to the experimental value.

The influence of the density functional and structural parameters on the predicted $a(Sc)$ values was also studied for a set of functionals implemented in the ORCA package, including two parametrizations of local density approximation (SVWN5[67] and PW[68]), GGA functionals BP,[62,66] BLYP, OLYP, PBE, and its two modifications ("revised PBE" (revPBE)[69] and aforementioned mPBE), meta-GGA functional TPSS,[70] as well as two

hybrid functionals, B3LYP and TPSSh[71] (the latter includes 10% of exact exchange). Point energy calculations were performed at the PBE/TZ2P and B3LYP/6-311G*-optimized coordinates using the cc-pwCVTZ basis set for Sc and 6-311G* for C and N atoms. Results of these calculations (Table 4) confirm conclusions given above. A systematic increase of $a(Sc)$ by ∼6 G can be seen when PBE/TZ2P-optimized coordinates are replaced by those optimized at the B3LYP/6-311G* level. $a(Sc)$ values predicted by GGA functionals (except for OLYP) are found in 25−35 G range, the largest value (34.09 G) provided by the BP functional. TPSS-predicted $a(Sc)$ also falls in this interval, while inclusion of the exact exchange term results in a slight increase of $a(Sc)$. Surprisingly, the largest $a(Sc)$ value is predicted in the framework of LSDA.

Inclusion of the scalar-relativistic terms in the framework of regular approximation increases DFT-predicted $a(Sc)$ values as already found for the SRD approach. In particular, ZORA results in a modest increase of $a(Sc)$ by 1−2 G, IORA yields higher increases of $a(Sc)$ (up +5.5 G for TPSS and +5.4 G for TPSSh), while MIORA-predicted values always fall between those of ZORA and IORA. Consideration of the spin−orbit interactions results in the slight decrease of $a(Sc)$ (by −0.2−0.3 G), which is in line with the small influence of this effect for relatively light Sc atoms as found earlier.[72] Note that predicted values of g-factor (Table 4) are found to be in reasonable agreement with the experimental values (1.9984(2)[23] and 1.9959[14]).

To our knowledge, before this work, there was only one report on DFT calculations of $Sc_3N@C_{80}$ in anionic state. Jakes et al.[23] reported RO-B3LYP/3-21G* and RO-HF calculations for $Sc_3N@C_{80}^-$ suggesting C_{3v} symmetry of the latter, and found surprisingly small $a(Sc)$ hfc of 7.14 and 14.27 G, respectively. The authors also reported that an increase of the basis set to 6-31G* did not result in significant changes of predicted values.

In summary, a correct prediction of $a(Sc)$ hfc in $Sc_3N@C_{80}^-$ appears to be a challenge for modern DFT theory. A successive increase of the complexity of the computational approach in terms of the basis set and density functional, as well as

(67) Vosko, S. H.; Wilk, L.; Nusair, M. *Can. J. Phys.* **1980**, *58* (8), 1200–1211.
(68) Perdew, J. P.; Wang, Y. *Phys. Rev. B* **1992**, *45* (23), 13244–13249.
(69) Zhang, Y.; Yang, W. *Phys. Rev. Lett.* **1998**, *80* (4), 890.
(70) Tao, J.; Perdew, J. P.; Staroverov, V. N.; Scuseria, G. E. *Phys. Rev. Lett.* **2003**, *91* (14), 146401.

(71) Staroverov, V. N.; Scuseria, G. E.; Tao, J.; Perdew, J. P. *J. Chem. Phys.* **2003**, *119* (23), 12129–12137.
(72) Remenyi, C.; Reviakine, R.; Arbuznikov, A. V.; Vaara, J.; Kaupp, M. *J. Phys. Chem. A* **2004**, *108* (23), 5026–5033.

consideration of relativistic corrections, results in the increase of the predicted value, but all predicted values are still too small to explain the experimental results.

Spin-Charge Separation in $Sc_3N@C_{80}^-$ and Cluster−Cage Interactions. The studies of the spin density distribution in $Sc_3N@C_{80}^-$ anion revealed an interesting peculiarity of the cluster charge state in the clusterfullerene anions. Both the Mulliken population analysis as well as the Bader analysis of the electron density topology show that there is only a slight decrease of the cluster charge in the anions as compared to that in the neutral state, in spite of a dominating cluster contribution to the spin density. For instance, while the spin population of 0.64 is found on the cluster in C_{3v}-$Sc_3N@C_{80}^-$, the net Bader charge of the cluster decreases by only $0.16e$, from $+3.52$ in $Sc_3N@C_{80}$ to $+3.36$ in $Sc_3N@C_{80}^-$. Furthermore, the difference of the net cluster charges in C_{3v}-$Sc_3N@C_{80}^-$ and C_{3v}-$Sc_3N@C_{80}^{2-}$ is only $0.09e$. Other conformers of $Sc_3N@C_{80}^-$ have a smaller spin population on the cluster, and the difference of the net cluster charges in the neutral and anionic forms is even smaller than in the C_{3v} conformer (Table 2). Thus, there is an apparent paradox as the small change of the cluster charge contradicts the localization of the LUMO (SOMO) and the spin density on the cluster. To clarify the mechanism of this spatial spin−charge separation in $Sc_3N@C_{80}^-$, we have to review first the bonding situation in the neutral $Sc_3N@C_{80}$.

The bond formation between the species such as the fullerene cage and the encapsulated cluster can be conveniently visualized by plotting the difference density,[8,10,73] i.e. the changes in the electron density (ED) distribution $\Delta\rho = [\rho(\text{Mol}) - \rho(\text{ref})]$, where $\rho(\text{Mol})$ is ED in the molecule under study, while $\rho(\text{ref})$ is the ED of the reference system (in which atomic coordinates are constrained to those of the studied molecule). As cluster−cage interactions are formally described by the 6-fold electron transfer from the cluster to the cage, it seems convenient to analyze two reference systems: one comprising the neutral noninteracting C_{80} cage and Sc_3N cluster (the difference density obtained with respect to this reference system is denoted hereafter as $\Delta\rho_{\text{neutr}}$), and the other one comprising noninteracting C_{80}^{6-} and M_3N^{6+} ions (the corresponding difference density is denoted hereafter as $\Delta\rho_{\text{ion}}$). $\Delta\rho_{\text{neutr}}$ describes the density redistribution caused by the electron transfer and bond formation, while $\Delta\rho_{\text{ion}}$ visualizes in which respect the actual cluster-to-cage electron transfer is different from six electrons and hence in which respect the cluster−cage interaction is different from being purely ionic.

The $[\rho(C_{80}^{6-}) - \rho(C_{80})]$ difference, $\Delta\rho_{\text{neutr}}$, and $\Delta\rho_{\text{ion}}$ for C_{3v}-$Sc_3N@C_{80}$ are shown in Figure 5. It can be seen that, while the surplus electrons in C_{80}^{6-} are distributed over the cage almost uniformly and without any preferable localization sites (Figure 5a), the situation is much different in $Sc_3N@C_{80}$. Figure 5b shows that the depletion of the density (i.e., region with negative $\Delta\rho_{\text{neutr}}$) is primarily anchored to Sc atoms and localized along the direction of the Sc−N bonds both between Sc and N and between Sc and the carbon cage. On the side of the carbon cage, the lobe of the negative $\Delta\rho_{\text{neutr}}$ is surrounded by the region with positive $\Delta\rho_{\text{neutr}}$. The latter is primarily localized *inside* the cage between the carbon atoms and the metal, while the fraction of $\Delta\rho_{\text{neutr}}$ outside the cage and on the carbon atoms which are not coordinated to the metals is very small. Positive $\Delta\rho_{\text{neutr}}$ also forms a toroid around the Sc atoms, which is in turn surrounded by a toroid with the negative $\Delta\rho_{\text{neutr}}$. Thus, the cluster−cage interaction in $Sc_3N@C_{80}$ has a much more complex nature than

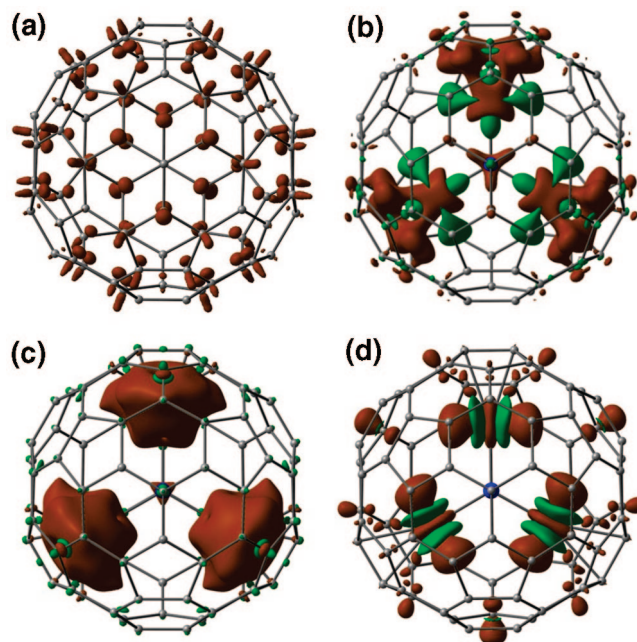(73) Wu, J.; Hagelberg, F. *J. Phys. Chem. C* **2008**, *112* (15), 5770−5777.

Figure 5. Difference densities of C_{3v}-$Sc_3N@C_{80}$: (a) $[\rho(C_{80}^{6-}) - \rho(C_{80})]$; (b) $[\rho(Sc_3N@C_{80}) - \rho(C_{80}) - \rho(Sc_3N)]$; (c) $[\rho(Sc_3N@C_{80}) - \rho(C_{80}^{6-}) - \rho(Sc_3N^{6+})]$; (d) $[\rho(Sc_3N@C_{80}^-) - \rho(Sc_3N@C_{80})]$. (a−c) are plotted with an isodensity value of 0.008 au, (d) is plotted with an isodensity value of 0.0016 au; brown denotes regions with positive $\Delta\rho$, green denotes regions with negative $\Delta\rho$. All coordinates are constrained to those of B3LYP/6-311G*-optimized C_{3v}-$Sc_3N@C_{80}^-$. One should not be confused by the "absence" of the negative part of the difference density in (c). Small contributions from the cage carbon atoms are evenly distributed over the cage and are not seen with the used isodensity value. See Figure S4 (Supporting Information) for the $[\rho(Sc_3N@C_{80}) - \rho(C_{80}^{6-}) - \rho(Sc_3N^{6+})]$ plotted with different isodensity values.

just an electron transfer from Sc atoms to the carbon cage would have. A significant degree of covalency in the cluster−cage interaction is obviously present. Importantly, the $\Delta\rho_{\text{neutr}}$ pattern shown in Figure 5b for $Sc_3N@C_{80}$ is very similar to that of $\Delta\rho_{\text{neutr}}$ reported by Campanera et al.[8] for $Sc_3N@C_{78}$. Our calculations also show that $\Delta\rho_{\text{neutr}}$ and $\Delta\rho_{\text{ion}}$ in $Sc_3N@C_{80}$, $Sc_3N@C_{68}$, and $Sc_3N@C_{78}$ are virtually identical (see Figure S3 in Supporting Information for $\Delta\rho_{\text{neutr}}$ and $\Delta\rho_{\text{ion}}$ patterns in $Sc_3N@C_{68}$ and $Sc_3N@C_{78}$ computed in this work). Thus, there is no significant difference between the mechanisms of the cluster−cage bonding in all three clusterfullerenes, and the postulate of the "weak" cluster−cage bonding in $Sc_3N@C_{80}$ based on the free rotation of the cluster on the NMR time scale and small relative energies of different conformers, as opposed to the strong bonds and fixed cluster in $Sc_3N@C_{68}$ and $Sc_3N@C_{78}$, should be revised. The reason of the almost free cluster rotation in $Sc_3N@C_{80}$ is the availability of multiple equal bonding sites so that the cluster can jump between them without a significant barrier. However, at each bonding site the cluster establishes a strong bonding with the carbon cage as revealed by vibrational spectroscopy[45,49] which has a significantly higher time resolution than NMR spectroscopy.

Covalent contributions to the cluster−cage bonding in $Sc_3N@C_{80}$ can be emphasized by the analysis of the spatial distribution of $\Delta\rho_{\text{ion}}$. If ionic C_{80}^{6-} and Sc_3N^{6+} species are set to interact with each other, a redistribution of ED occurs, including the cage-to-cluster electron transfer and concentration of the electron density *between* the Sc atoms and the cage (Figure 5c). Such a concentration can be regarded as a clear

Table 5. Bader and Mulliken Charges of the Metal Atoms (q(M)) and Net Cluster Charges (q(cluster)) in the Neutral and Anionic State of Selected Endohedral Fullerenes, and Cluster Spin Population in Radical Species

	$q = 0$				$q = -1$				
	q(M), Bader	q(M), Mulliken	q(cluster), Bader	q(cluster), Mulliken	q(M), Bader	q(M), Mulliken	Δq(cluster), Bader	Δq(cluster), Mulliken	cluster spin population
C_{3v}-$Y_3N@C_{80}$	1.88	1.38	3.75	2.65	1.85	1.39	−0.09	0.02	0.29
C_s-$Y_3N@C_{80}$	1.86, 1.88 (x2)	1.44, 1.42 (x2)	3.78	2.67	1.86, 1.86 (x2)	1.46 1.43 (x2)	−0.04	0.06	0.15
D_3-$Y_3N@C_{80}$	1.88	1.43	3.79	2.68	1.88	1.46	−0.01	0.09	0.06
$Sc_3C_2@C_{80}$[a]	1.60, 1.65 (x2)	1.19, 1.18 (x2)	3.35	2.50	1.64, 1.65 (x2)	1.23 1.20 (x2)	−0.11	−0.03	0.89
$Ti_2C_2@C_{78}$	1.70	0.86	2.24	0.78	1.69	0.92	−0.03	0.09	0.53
$La_2@C_{72}$	1.87	1.80	3.75	3.60	1.66	1.64	−0.42	−0.32	1.01
$La_2@C_{78}$	1.82	1.79	3.65	3.58	1.64	1.66	−0.37	−0.25	0.95
$La_2@C_{80}$	1.77	1.78	3.54	3.55	1.64	1.69	−0.26	−0.18	0.96

[a] For $Sc_3C_2@C_{80}$, the values for $Sc_3C_2@C_{80}^+$ are given in $q = 0$ part of the table, while the values for the noncharged $Sc_3C_2@C_{80}$ are given in $q = -1$ part of the table.

manifestation of the covalency in the cluster−cage interactions. However, it is also obvious from Figure 5b and c that cluster−cage bonds are not localized (such as, e.g., carbon−carbon bonds) but can be better described by "coordination" bonds such as those found in transition metal complexes (e.g., ferrocene[74]). Atomic charges calculated in the framework of Bader's atoms-in-molecule theory show that approximately 2.5 electrons are transferred from C_{80}^{6-} to the cluster (i.e., the net cluster charge is +3.52). Other partition methods also predict that the cluster charge in $Sc_3N@C_{80}$ is substantially smaller than +6, the actual values varying between these approaches. For instance, net Mulliken and NBO charges of the Sc_3N cluster computed in this work are +2.88 and +2.99; Valencia et al.[75] reported the net Sc_3N charges of +1.28 (Mulliken), +1.10 (Hirshfeld), +0.94 (Voronoi).[76] Importantly, the occupation of the 4s(Sc) orbitals in $Sc_3N@C_{80}$ is very small, i.e. the covalent cluster−cage bonding occurs through the $d_{Sc}−\pi_{cage}$ interactions.

In summary, the mechanism of cluster−cage interaction in $Sc_3N@C_{80}$ can be described by the formal transfer of six electrons from the cluster to the cage with a subsequent coordination of Sc cations by the cage as a "ligand" and reoccupation of Sc 3d orbitals (see also ref 10 for more detailed discussion). Note that there are no special localized orbitals that could be responsible for the cage-to-cluster electron transfer. Instead, this kind of interaction occurs through the overlap of many cage π-orbitals with 3d orbitals of Sc. This scheme provides a simple explanation of how the spatial separation of the spin and the charge occurs in $Sc_3N@C_{80}^-$. The LUMO in $Sc_3N@C_{80}$ is presumably localized on the cluster and built by the linear combination of 3d(Sc) orbitals. If then an additional electron is added to $Sc_3N@C_{80}$, it should formally increase the population of 3d(Sc) orbitals, but eventually this also leads to the decrease of the of $d_{Sc}−\pi_{cage}$ overlap so that overall 3d(Sc) population is not significantly altered. As a result, while the spin on $Sc_3N@C_{80}^-$ resides on the cluster in the same degree as the LUMO is localized there, the charge state of the cluster is not affected in the same way, the negative charge being delocalized over the cage; the increase of the barrier to the cluster rotation should be probably attributed to the increased Coulombic cluster−cage interaction. This effect can be visual-ized by plotting the $[\rho(Sc_3N@C_{80}^-) - \rho(Sc_3N@C_{80})]$ difference density regarded hereafter as $\Delta\rho_{-/0}$ (Figure 5d). For conventional ion radicals, in which spin and charge are not spatially separated, $\Delta\rho_{-/0}$ should have similar shape to the spin density (and the density of LUMO/SOMO). However, for the $Sc_3N@C_{80}^-$ anion radical it can be clearly seen that the lobes of the positive part of $\Delta\rho_{-/0}$, which indeed resemble the spin density distribution in $Sc_3N@C_{80}^-$ (Figure 4a), are superimposed with the lobes of the negative part of $\Delta\rho_{-/0}$, which are anchored to the Sc atoms and which compensate the extra negative charge. Such a charge distribution in $Sc_3N@C_{80}^-$ explains why X-ray electron spec-troscopy[6] did not reveal considerable changes in the population of Sc 3d orbitals in K-doped $Sc_3N@C_{80}$ as compared to the undoped $Sc_3N@C_{80}$ in spite of formal localization of the surplus electron on the cluster revealed by ESR spectroscopy of the $Sc_3N@C_{80}^-$ anion radical.[23]

Spin−Charge Separation as a General Rule for Endohedral Fullerenes with Metal-Based LUMO. The mech-anism of the charge−spin separation in $Sc_3N@C_{80}^-$ implies that this phenomenon can be expected for those endohedral clus-terfullerenes which exhibit a similar type of cluster−cage bonding and have their LUMO (SOMO in the anions) localized on the cluster. To verify this suggestion, we have analyzed a broad range of endohedral fullerenes, including nitride cluster-fullerenes, carbide clusterfullerenes, and dimetallofullerenes (Table 5 and Figure S6 [Supporting Information]).

Sc-Based Nitride Clusterfullerenes. In addition to $Sc_3N@C_{80}$, the Sc-based nitride clusterfullerene family also includes $Sc_3N@C_{68}$,[77,78] $Sc_3N@C_{70}$[79] and $Sc_3N@C_{78}$.[80] A spectroelec-trochemical study of $Sc_3N@C_{68}$ augmented by DFT calcula-tions[81] has recently shown that the spin density in $Sc_3N@C_{68}^-$ is delocalized over the cage with a small cluster contribution. A presumable localization of the spin density on the carbon cage was also found in this work for $Sc_3N@C_{70}^-$. The situation with $Sc_3N@C_{78}$ is more complex. Our B3LYP calculations have shown that the LUMO of $Sc_3N@C_{78}$ is localized on the cluster and is similar to that in C_{3v}-$Sc_3N@C_{80}$ (Figure 6), which agrees

(74) Cortés-Guzmán, F.; Bader, R. F. W. *Coord. Chem. Rev.* **2005**, *249* (5−6), 633−662.

(75) Valencia, R.; Rodríguez-Fortea, A.; Poblet, J. M. *J. Phys. Chem. A* **2008**, *112* (20), 4550−4555.

(76) Note that Mulliken charges calculated in this work at the B3LYP/ 6-311G* level and those from ref 75 calculated using BP functional and triple-ζ basis set with ZORA relativistic corrections are substantially different, pointing to the strong dependence of Mulliken charges to the method of theory used.

(77) Stevenson, S.; Fowler, P. W.; Heine, T.; Duchamp, J. C.; Rice, G.; Glass, T.; Harich, K.; Hajdu, E.; Bible, R.; Dorn, H. C. *Nature* **2000**, *408* (6811), 427−428.

(78) Yang, S. F.; Kalbac, M.; Popov, A.; Dunsch, L. *Chem. Eur. J.* **2006**, *12* (30), 7856−7863.

(79) Yang, S. F.; Popov, A. A.; Dunsch, L. *Angew. Chem., Int. Ed.* **2007**, *46* (8), 1256−1259.

(80) Olmstead, M. H.; de Bettencourt-Dias, A.; Duchamp, J. C.; Stevenson, S.; Marciu, D.; Dorn, H. C.; Balch, A. L. *Angew. Chem., Int. Ed.* **2001**, *40* (7), 1223−1225.

(81) Rapta, P.; Popov, A. A.; Yang, S. F.; Dunsch, L. *J. Phys. Chem. A* **2008**, *112*, 5858−5865.
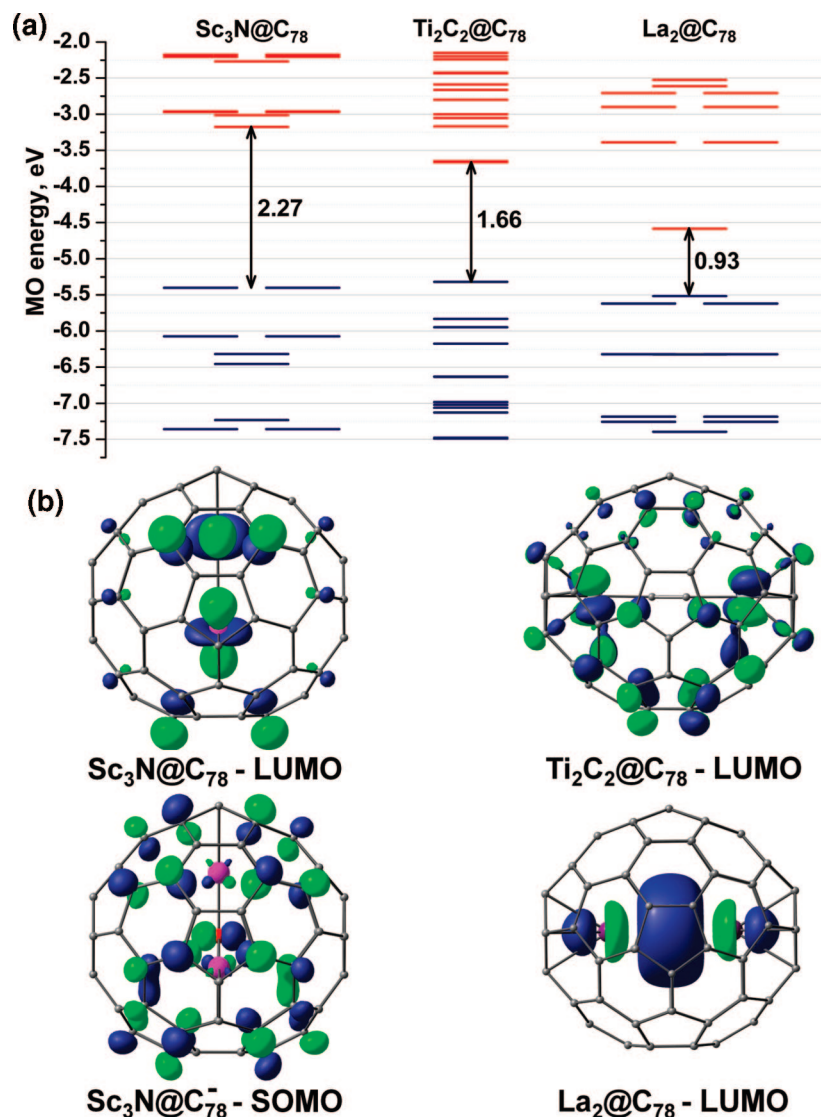
Figure 6. (a) MO energy levels in $Sc_3N@C_{78}$, $Ti_2C_2@C_{78}$, and $La_2@C_{78}$ all based on C_{78}-D_{3h}(5) carbon cage, as obtained at the B3LYP//PBE level. (b) LUMO in $Sc_3N@C_{78}$, $Ti_2C_2@C_{78}$, and $La_2@C_{78}$ and SOMO in $Sc_3N@C_{78}^-$. MOs are plotted with isodensity value of 0.035 au. SOMO in $Ti_2C_2@C_{78}^-$ and $La_2@C_{78}^-$ are virtually identical to LUMOs of the neutrally charged species and thus are not shown.

with previous calculations with GGA functionals.[8,9] However, LUMO+1, which is primarily localized on the carbon cage, is very close in its energy to the LUMO, and in the $Sc_3N@C_{78}^-$ the order of LUMO and LUMO+1 is inversed so that SOMO is based on the LUMO+1 of the neutrally charged $Sc_3N@C_{78}$ (Figure 6). As a result, the spin density in $Sc_3N@C_{78}$ is localized on the cage, the net cluster spin population being less than 0.01. In the view of the small energy gap between the two orbitals, a conclusion based on DFT calculations cannot be considered as definitive and further experimental studies of this nitride clusterfullerene are necessary.

Y-Based Nitride Clusterfullerenes. Y-Based nitride clusterfullerenes, as well as those with lanthanide atoms, can be formally described as $M_3N^{6+}@C_{2n}^{6-}$, just like their Sc counterparts. In spite of the similarity with Sc-based nitride clusterfullerenes, it was found that $Y_3N@C_{80}$ and other $M_3N@C_{80}$ clusterfullerenes (M = lanthanide) show a weak but salient variation in their electronic structure, manifested in somewhat different UV−vis absorption spectra, the shift of the vibrational frequencies of the carbon cage modes, increased cluster−cage force constant, and shifted redox potentials as compared to those

of $Sc_3N@C_{80}$.[13,49,82,83] Recently, these phenomena were attributed to the higher cluster-to-cage electron transfer in $M_3N@C_{80}$ (M = Y, lanthanides) than in $Sc_3N@C_{80}$.[49] Analysis of the Bader charges evaluated in this work indeed shows that the net charge of the Y_3N cluster in C_3-$Y_3N@C_{80}$, +3.78, is by 0.25 larger than the charge of Sc_3N in C_3-$Sc_3N@C_{80}$, +3.53 (Table 5). In particular, the charge on Y atoms is +1.88 (vs +1.77 on Sc), while the nitrogen atom in $Y_3N@C_{80}$ bears a more negative charge (−1.85) than in $Sc_3N@C_{80}$ (−1.77).

Due to the larger cluster size, rotation of Y_3N in $Y_3N@C_{80}$ was suggested to be more hindered than that of Sc_3N in $Sc_3N@C_{80}$,[43] and this is further confirmed by our calculations as shown in Figure 2a. At the PBE/TZ2P level, the C_3 conformer is found to be a ground state of $Y_3N@C_{80}$, followed by the C_s-conformer ($\Delta E = 8.8$ kJ/mol). The C_{3v} conformer is much higher in energy (21.6 kJ/mol) and is not an energy minimum in $Y_3N@C_{80}$ (Figure 2a); the cluster in this structure is

(82) Dunsch, L.; Krause, M.; Noack, J.; Georgi, P. *J. Phys. Chem. Solids* **2004**, *65* (2−3), 309–315.
(83) Yang, S. F.; Popov, A. A.; Kalbac, M.; Dunsch, L. *Chem. Eur. J.* **2008**, *14* (7), 2084–2092.

substantially pyramidal (the nitrogen is displaced out of the Y_3 plane by 0.470 Å), which is an indication of the strong strain caused by the insufficient size of the cage. Note that in comparison to $Sc_3N@C_{80}$, C_3-$Y_3N@C_{80}$ has a larger value of the cluster rotation angle φ (22.5° for Y_3N vs 18.1° for Sc_3N), while the relative energy of the conformer with $\varphi = 30°$ is only 2.3 kJ/mol (in $Y_3N@C_{80}$ this conformer has C_3 symmetry because of the slight pyramidalization of the cluster, while in $Sc_3N@C_{80}$ rigorous D_3 symmetry is present). In the anionic form, the order of the conformers is preserved, and the most stable structure is still the C_3 conformer. However, relative energies of both the C_s and C_{3v} conformers are reduced as compared to the neutral $Y_3N@C_{80}$, and the true energy minimum is developed for the C_{3v} conformer (see Figure S5 in Supporting Information for the section of potential energy surface along φ in $Y_3N@C_{80}^-$). Point energy B3LYP/(6-311G*,TZVPP) calculations at the PBE/TZ2P-optimized coordinates predict that the conformer with $\varphi = 30°$ is more stable than the C_3-conformer ($\varphi = 25.5$), while the relative energy of the C_{3v} conformer is further reduced ($\Delta E = 12.9$ kJ/mol at the B3LYP//PBE level vs 16.2 kJ/mol at the PBE level).

The spin density distribution in C_{3v}, C_s, and D_3 conformers of $Y_3N@C_{80}^-$ is compared to the spin density distribution in analogous conformers of $Sc_3N@C_{80}^-$ in Figure 4. Obviously the difference in the electronic structures of $Sc_3N@C_{80}$ and $Y_3N@C_{80}$ appears here as well, the spin densities on the cluster in $Y_3N@C_{80}^-$ being much smaller than in $Sc_3N@C_{80}^-$. The largest spin population on the Y_3N cluster, 0.29, is found in the C_{3v} conformer (compare to 0.64 in $Sc_3N@C_{80}^-$), while the cluster spin population in D_3-$Y_3N@C_{80}^-$ is only 0.06 (compare to 0.40 in $Sc_3N@C_{80}^-$). In view of the smaller spin population, the effect of the spatial spin–charge separation is less pronounced in $Y_3N@C_{80}^-$ than in $Sc_3N@C_{80}^-$; however, a substantially smaller change of the cluster charge (Bader analysis yields −0.09 for C_{3v} and −0.01 for D_3 conformers) compared to the spin population still can be pointed out. Interestingly, Mulliken analysis even shows an increase of the cluster size after accepting the electron. Note that the spin density at the Y nuclei in C_{3v}-$Y_3N@C_{80}^-$, 0.103 au (B3LYP//PBE level), is close to the value for Sc in the C_{3v} conformer, 0.092 au (B3LYP/6-311G* level), in spite of the 2 times smaller spin population on Y_3N cluster. However, a much smaller nuclear magnetic moment of Y and its negative sign result in comparably small and negative $a(^{89}Y)$ values for $Y_3N@C_{80}^-$ not exceeding −8.1 G for the C_{3v} conformer at the B3LYP//PBE level. A larger value, −15.5 G, is predicted for the same conformer at the SRD-PBE/Λ11 level.

The family of $Y_3N@C_{2n}$ clusterfullerenes considered here for calculations also includes $Y_3N@C_{2n}$ with $2n = 78, 82, 84, 86$, and 88. The structures of $Tb_3N@C_{2n}$ ($2n = 84, 86$, and 88) were established by single-crystal X-ray diffraction[84,85] and are believed to be the same for Y and all lanthanides. A recent single crystal X-ray diffraction study of $Gd_3N@C_{84}$ and $Tm_3N@C_{84}$ indeed confirmed that they are isostructural to $Tb_3N@C_{84}$ and

are based on the non-IPR C_s: 51565 isomer of C_{84}.[86] The structure of $M_3N@C_{78}$ based on the non-IPR C_2: 22010 cage isomer was recently suggested by our group based on DFT calculations and spectroscopic studies of $Tm_3N@C_{78}$ and $Dy_3N@C_{78}$,[87] while the non-IPR structure of $M_3N@C_{82}$ (C_s: 39663) was recently proved for $Gd_3N@C_{82}$ by a single-crystal X-ray study.[88] DFT calculations have shown that none of the studied $Y_3N@C_{2n}^-$ anions has significant spin population on the cluster atoms (see Figure S6 in Supporting Information for the plots with spatial distribution of their spin density).

Carbide Clusterfullerenes. The first carbide clusterfullerene was discovered in 2001 by Wang et al.,[89] and further studies have shown that some well-known endohedral metallofullerenes such as $Ti_2@C_{80}$, $Sc_3@C_{82}$, and major isomers of $Sc_2@C_{84}$ and $Y_2@C_{84}$ had to be reassigned to $Ti_2C_2@C_{78}$,[90,91] $Sc_3C_2@C_{80}$,[92] $Sc_2C_2@C_{82}$,[93,94] and $Y_2C_2@C_{82}$[95] carbide clusterfullerenes, respectively. Recently a new, non-IPR carbide clusterfullerene $Sc_2C_2@C_{68}$ was reported by Wang et al.[96] In these molecules the C_2 unit is believed to have a formal charge of −2,[75,91] and with the three-valence metal the whole M_2C_2 cluster has the formal charge of +4. Our calculations for the anions of $M_2C_2@C_{82}$ (M = Sc, Y) and $Sc_2C_2@C_{68}$ have shown that the spin density on the metal-carbide cluster in these anions is negligible, and hence these anions will not be considered hereafter (see Figure S6 in Supporting Information for the spatial distribution of the spin density; note that opposed to results of this work, Valencia et al.[75] reported significant localization of spin density on the Sc_2C_2 cluster in $Sc_2C_2@C_{82}^-$ at the BP86/TZP level). On the contrary, $Sc_3C_2@C_{80}$ and $Ti_2C_2@C_{78}$ are found to be suitable molecules to study the effect of the spatial charge–spin separation.

$Sc_3C_2@C_{80}$ is a special member of carbide clusterfullerene family as it is a radical in the neutral state.[97] Tan and Lu have shown that a formal charge distribution in $Sc_3C_2@C_{80}$ can be described as $(Sc^{3+})_3(C_2)^{3-}@C_{80}^{6-}$.[98] The same authors performed BLYP/DNP calculations of different redox states of $Sc_3C_2@C_{80}$ and showed that the oxidation and reduction results

(84) Beavers, C. M.; Zuo, T. M.; Duchamp, J. C.; Harich, K.; Dorn, H. C.; Olmstead, M. M.; Balch, A. L. *J. Am. Chem. Soc.* **2006**, *128* (35), 11352–11353.

(85) Zuo, T. M.; Beavers, C. M.; Duchamp, J. C.; Campbell, A.; Dorn, H. C.; Olmstead, M. M.; Balch, A. L. *J. Am. Chem. Soc.* **2007**, *129* (7), 2035–2043.

(86) Zuo, T.; Walker, K.; Olmstead, M. M.; Melin, F.; Holloway, B. C.; Echegoyen, L.; Dorn, H. C.; Chaur, M. N.; Chancellor, C. J.; Beavers, C. M.; Balch, A. L.; Athans, A. J. *Chem. Commun.* **2008**, *(9)*, 1067–1069.

(87) Popov, A. A.; Krause, M.; Yang, S. F.; Wong, J.; Dunsch, L. *J. Phys. Chem. B* **2007**, *111* (13), 3363–3369.

(88) Mercado, B. Q.; Beavers, C. M.; Olmstead, M. M.; Chaur, M. N.; Walker, K.; Holloway, B. C.; Echegoyen, L.; Balch, A. L. *J. Am. Chem. Soc.* **2008**, *130* (25), 7854–7855.

(89) Wang, C. R.; Kai, T.; Tomiyama, T.; Yoshida, T.; Kobayashi, Y.; Nishibori, E.; Takata, M.; Sakata, M.; Shinohara, H. *Angew. Chem., Int. Ed.* **2001**, *40* (2), 397–399.

(90) Yumura, T.; Sato, Y.; Suenaga, K.; Iijima, S. *J. Phys. Chem. B* **2005**, *109* (43), 20251–20255.

(91) Tan, K.; Lu, X. *Chem. Commun.* **2005**, *(35)*, 4444–4446.

(92) Iiduka, Y.; Wakahara, T.; Nakahodo, T.; Tsuchiya, T.; Sakuraba, A.; Maeda, Y.; Akasaka, T.; Yoza, K.; Horn, E.; Kato, T.; Liu, M. T. H.; Mizorogi, N.; Kobayashi, K.; Nagase, S. *J. Am. Chem. Soc.* **2005**, *127* (36), 12500–12501.

(93) Iiduka, Y.; Wakahara, T.; Nakajima, K.; Tsuchiya, T.; Nakahodo, T.; Maeda, Y.; Akasaka, T.; Mizorogi, N.; Nagase, S. *Chem. Commun.* **2006**, *(19)*, 2057–2059.

(94) Iiduka, Y.; Wakahara, T.; Nakajima, K.; Nakahodo, T.; Tsuchiya, T.; Maeda, Y.; Akasaka, T.; Yoza, K.; Liu, M. T. H.; Mizorogi, N.; Nagase, S. *Angew. Chem., Int. Ed.* **2007**, *46* (29), 5562–5564.

(95) Inoue, T.; Tomiyama, T.; Sugai, T.; Shinohara, H. *Chem. Phys. Lett.* **2003**, *382* (3–4), 226–231.

(96) Shi, Z. Q.; Wu, X.; Wang, C. R.; Lu, X.; Shinohara, H. *Angew. Chem., Int. Ed.* **2006**, *45* (13), 2107–2111.

(97) Shinohara, H.; Inakuma, M.; Hayashi, N.; Sato, H.; Saito, Y.; Kato, T.; Bandow, S. *J. Phys. Chem.* **1994**, *98* (35), 8597–8599.

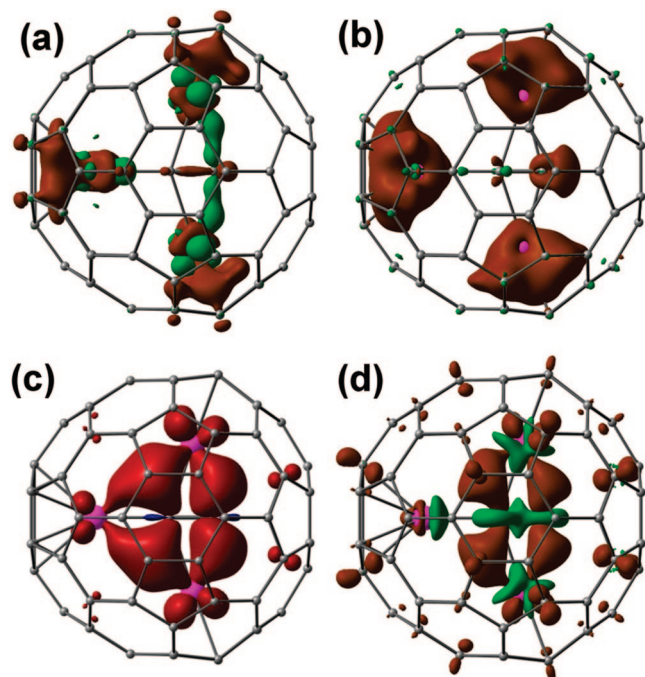(98) Tan, K.; Lu, X. *J. Phys. Chem. A* **2006**, *110* (3), 1171–1176.

Figure 7. Difference densities of $Sc_3C_2@C_{80}$ carbide clusterfullerene: (a) $[\rho(Sc_3C_2@C_{80}) - \rho(C_{80}) - \rho(Sc_3C_2)]$; (b) $[\rho(Sc_3C_2@C_{80}) - \rho(C_{80}^{6-}) - \rho(Sc_3C_2^{6+})]$; (d) $[\rho(Sc_3C_2@C_{80}) - \rho(Sc_3C_2@C_{80}^{+})]$; (c) spin density in $Sc_3C_2@C_{80}$. (a) and (b) are plotted with isodensity value of 0.008 au, (c) and (d) are plotted with isodensity value of 0.0016 au; brown denotes regions with positive $\Delta\rho$, green denotes negative $\Delta\rho$. All coordinates are constrained to those of neutral $Sc_3C_2@C_{80}$.

Figure 8. Difference densities of the $Ti_2C_2@C_{78}$: (a) $[\rho(Ti_2C_2@C_{78}) - \rho(C_{78}) - \rho(Ti_2C_2)]$; (b) $[\rho(Ti_2C_2@C_{78}) - \rho(C_{78}^{6-}) - \rho(Ti_2C_2^{6+})]$; (d) $[\rho(Ti_2C_2@C_{78}^{-}) - \rho(Ti_2C_2@C_{78})]$; (c) spin density in $Ti_2C_2@C_{78}^{-}$. (a) and (b) are plotted with isodensity value of 0.008 au, (c) and (d) are plotted with isodensity value of 0.0016 au, brown denotes regions with positive $\Delta\rho$, green denotes negative $\Delta\rho$. The inset shows a fragment of $\Delta\rho_{-/0}$ viewed along the three-fold axis of the carbon cage.

in the change of the charge state of C_2 unit. The authors reported several conformers of $Sc_3C_2@C_{80}$ with different positions of the C_2 unit with respect to Sc atoms as well as different positions of the cluster as a whole with respect to the carbon cage. For our analysis, we have chosen the most stable C_{2v}-symmetric isomers from ref 98 which has a planar Sc_3C_2 cluster. However, our calculations at the PBE/TZ2P level have shown that this structure had one imaginary frequency, while the true minimum was obtained by displacing the central carbon atom in the Sc_3C_2 cluster by 0.348 Å out of the Sc_3 plane, so that actual symmetry of $Sc_3C_2@C_{80}$ studied in this work was C_s (at the PBE/ TZ2P level the C_s conformer is found to be 2.3 kJ/mol lower in energy than the C_{2v} conformer). In view of the free rotation of the C_2 unit in carbide clusterfullerenes,[99] small structural variations of the energy minima of $Sc_3C_2@C_{80}$ predicted by different methods are not surprising.

Figure 7 shows the $\Delta\rho_{neutr}$ and $\Delta\rho_{ion}$ distribution for $Sc_3C_2@C_{80}$ computed in this work, which is found to be quite similar to that of $Sc_3N@C_{80}$, except for the small but non-negligible contribution of one of the carbon atoms apparent for both types of difference density in $Sc_3C_2@C_{80}$. For B3LYP// PBE computed electron density, Bader analysis yields the charge of -1.69 for the C_2 unit and $+1.65$ for each Sc atom (compare to the Sc charges of $+1.76$ in $Sc_3N@C_{80}$) so that the net charge of the Sc_3C_2 cluster is $+3.24$. The Mulliken spin population of the cluster is 0.89 (see also Figure 7); of that, 0.42 is due to the C_2 unit, two symmetric Sc atoms each bear 0.20, while the spin population for the Sc atom on the symmetry plane is 0.07 (see
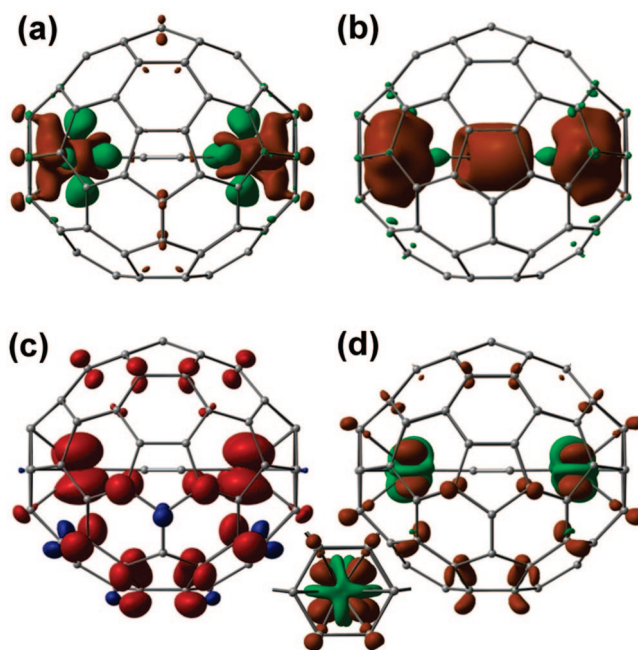
Figure 7 for the spatial distribution of spin density in $Sc_3C_2@C_{80}$). In accordance with the results of Tan and Lu[98] as well as the results of this work showing an exclusive localization of the SOMO on the cluster, the addition or removal of one electron to/from $Sc_3C_2@C_{80}$ should result in the change of the cluster charge by one unit. However, the net charge of the Sc_3C_2 cluster in $Sc_3C_2@C_{80}^{+}$ is $+3.35$; i.e. by addition of one electron to $Sc_3C_2@C_{80}^{+}$ the cluster charge is changed by only -0.11 (Table 5). Figure 6d shows the spatial distribution of $[\rho(Sc_3C_2@C_{80}) - \rho(Sc_3C_2@C_{80}^{+})]$ difference density, which is similar to the spin density but exhibits a significant depletion of the density on the Sc atoms and the C_2 unit. Likewise, addition of one electron to $Sc_3C_2@C_{80}$ changes the net cluster charge by -0.34. Thus, when the cluster-based LUMO in $Sc_3C_2@C_{80}^{+}$ is populated by *two* electrons, the charge of the cluster by only -0.45, which shows that the charge–spin separation occurs in $Sc_3C_2@C_{80}$ similar to that in $Sc_3N@C_{80}^{-}$.

The formal charge distribution in $Ti_2C_2@C_{78}$ can be described as $(Ti^{4+})_2C_2^{2-}@C_{78}^{6-}$, and this clusterfullerene is distinguished by the strong covalent interactions suggested between Ti and the carbon cage found in earlier DFT calculations as well as UPS studies.[90,91,100] Different conformers originating from the rotation of the C_2 unit were reported earlier for this molecule.[90,91] Our PBE/TZ2P calculations have shown that the structure with an almost linear Ti−C−C−Ti chain (Ti−C−C angle is 154°) and an overall C_2 symmetry has the lowest energy and has no imaginary frequencies, and this structure was adopted for the following analysis. Figure 8a shows the $\Delta\rho_{neutr}$ distribution for $Ti_2C_2@C_{78}$, which exhibits a similar pattern for Ti atoms as

(99) Krause, M.; Hulman, M.; Kuzmany, H.; Dubay, O.; Kresse, G.; Vietze, K.; Seifert, G.; Wang, C.; Shinohara, H. *Phys. Rev. Lett.* **2004**, *93* (13), 4.

(100) Hino, S.; Kato, M.; Yoshimura, D.; Moribe, H.; Umemoto, H.; Ito, Y.; Sugai, T.; Shinohara, H.; Otani, M.; Yoshimoto, Y.; Okada, S. *Phys. Rev. B* **2007**, *75* (12), 5.

already found for Sc in $Sc_3N@C_{80}$ (Figure 5) and $Sc_3C_2@C_{80}$ (Figure 7). The resulting $\Delta\rho_{ion}$ distribution calculated by using the superposition of the electron densities of noninteracting $C_{78}{}^{6-}$ and $Ti_2C_2{}^{6+}$ species as a reference exhibits a significant positive density both on Ti and the C_2 unit. Bader charges evaluated for B3LYP//PBE computed electron density are $+1.70$ for Ti and -0.58 for C, resulting in the charge of -1.16 for the C_2 unit and $+2.24$ for the whole cluster (Table 5).

As shown in Figure 6, the LUMO of $Ti_2C_2@C_{78}$ has a substantial contribution from Ti atoms and is lower in energy than the LUMO in $Sc_3N@C_{78}$, which has the same carbon cage (in fact, there are two quasi-degenerate orbitals with similar spatial distribution; they would be truly degenerate if the Ti−C−C−Ti chain were linear and the molecule had an overall D_{3h} symmetry). Addition of one electron to $Ti_2C_2@C_{78}$ results in a 0.27 spin population for each Ti atom and a negligible spin population for the C_2 unit. In spite of the spin localization on Ti atoms, Bader analysis of the electron density in $Ti_2C_2@C_{78}{}^-$ reveals a negligible change of -0.01 for Ti atomic charges as compared to the neutral $Ti_2C_2@C_{78}$, and the regions with negative $\Delta\rho_{-/0}$ are clearly seen in Figure 8d. Thus, the spatial charge−spin separation is found for the $Ti_2C_2@C_{78}{}^-$ anion.

Dimetallofullerenes. For the studies of the dimetallofullerenes, we have chosen $Y_2@C_{82}$,[101] $Sc_2@C_{76}$[101−103] and the family of $La_2@C_{2n}$ ($2n = 72$,[104,105] 78,[106] 80[107,108]). B3LYP//PBE calculations for $Y_2@C_{82}{}^-$ and $Sc_2@C_{76}{}^-$ have shown that their spin densities have little contributions from the metals, and hence these metallofullerenes will not be considered here (see Figure S6 for the spin density distribution in these anions).

Figure 6 shows the energies of the frontier orbitals in $La_2@C_{78}$ as compared to $Sc_3N@C_{78}$ and $Ti_2C_2@C_{78}$ all based on the same $D_{3h}(5)$ carbon cage isomer. The LUMO in $La_2@C_{78}$ is much lower in energy than LUMOs in clusterfullerenes, and opposed to the latter, LUMO (and SOMO in the respective anion) is spatially localized exclusively on the lanthanum atoms. Analogous La-localized low-energy LUMOs are found for $La_2@C_{72}$ and $La_2@C_{80}$, and thus they are responsible for the small optical bandgaps found for these dimetallofullerenes when compared to the clusterfullerenes with the same carbon cage and formal cage charges (e.g., $La_2@C_{78}$ vs $Sc_3N@C_{78}$ and $La_2@C_{80}$ vs $Sc_3N@C_{80}$).

Parts a and b of Figure 9 show the $\Delta\rho_{neutr}$ and $\Delta\rho_{ion}$ distribution for $La_2@C_{80}$ for which a D_{2h} conformer was chosen as it was predicted to have the lowest energy in the recent scalar-
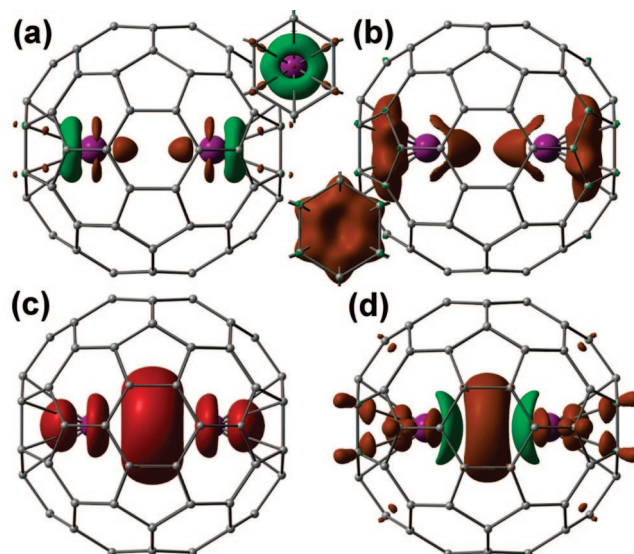

Figure 9. Difference densities of the D_{2h}-$La_2@C_{80}$: (a) $[\rho(La_2@C_{80}) - \rho(C_{80}) - \rho(La_2)]$; (b) $[\rho(La_2@C_{80}) - \rho(C_{80}{}^{6-}) - \rho(La_2{}^{6+})]$; (d) $[\rho(La_2@C_{80}{}^-) - \rho(La_2@C_{80})]$; (c) spin density in $La_2@C_{80}{}^-$. (a) and (b) are plotted with an isodensity value of 0.010 au; (c) and (d) are plotted with an isodensity value of 0.0016 au; brown denotes regions with positive $\Delta\rho$, green denotes negative $\Delta\rho$. The insets show fragments of $\Delta\rho_{neutr}$ and $\Delta\rho_{ion}$ viewed along the two-fold axis of the carbon cage. To construct $\Delta\rho_{neutr}$, La_2 dimer in the triplet state was used (rather then individual La atoms).

relativistic DFT studies[109] as well as in our PBE/TZ2P calculations. The $\Delta\rho_{neutr}$ distribution in $La_2@C_{80}$ is different from that in Sc- and Ti-clusterfullerenes, forming a torus of the density depletion between La and the cage hexagon as well as the region of positive $\Delta\rho_{neutr}$ on La and *between* two La atoms. The $\Delta\rho_{ion}$ distribution clearly shows that the electron density donated back to the La atoms is concentrated between the carbon cage and La, thus representing a covalent contribution to La-cage bonding. Partial concentration of the positive part of $\Delta\rho_{ion}$ density between two La atoms should be also pointed out as it can be an indication of the covalency in La···La interactions. Bader analysis of B3LYP//PBE densities reveals La charges of $+1.87$, $+1.82$, and $+1.77$ in $La_2@C_{72}$, $La_2@C_{78}$, and $La_2@C_{80}$, respectively (Table 5).

To get more insight into the possible degree of covalency in La···La interactions, we have used AIMAll code[110] to perform QTAIM analysis of the electronic density of D_{2h}-$La_2@C_{80}$ obtained at the B3LYP/(6-311G*, UGBS) level (the use of the full-electron basis set for La was mandatory for this analysis). Analysis of the topology of the electron density revealed a bond critical point (bcp) between two La atoms with a small value of the electronic density, $\rho_{bcp} = 0.09$ e Å^{-3}, and a small positive value of the density Laplacian, $\nabla^2\rho_{bcp} = 0.34$ e Å^{-5}. Note that a bcp with a small value of $\rho_{bcp} = 0.14$ e Å^{-3} and small negative $\nabla^2\rho_{bcp} = -0.02$ e Å^{-5} was also found by Kobayashi and Nagase between two Sc atoms in $Sc_2@C_{84}$.[111] In the framework of QTAIM, the nature of the interaction between the atoms can be revealed by the analysis of the values of certain descriptors

(101) Inoue, T.; Tomiyama, T.; Sugai, T.; Okazaki, T.; Suematsu, T.; Fujii, N.; Utsumi, H.; Nojima, K.; Shinohara, H. *J. Phys. Chem. B* **2004**, *108* (23), 7573−7579.
(102) Wang, C. R.; Georgi, P.; Dunsch, L.; Kai, T.; Tomiyama, T.; Shinohara, H. *Curr. Appl. Phys.* **2002**, *2* (2), 141−143.
(103) Popov, A. A.; Dunsch, L. *J. Am. Chem. Soc.* **2007**, *129* (38), 11835−11849.
(104) Stevenson, S.; Burbank, P.; Harich, K.; Sun, Z.; Dorn, H. C.; van Loosdrecht, P. H. M.; deVries, M. S.; Salem, J. R.; Kiang, C. H.; Johnson, R. D.; Bethune, D. S. *J. Phys. Chem. A* **1998**, *102* (17), 2833−2837.
(105) Kato, H.; Taninaka, A.; Sugai, T.; Shinohara, H. *J. Am. Chem. Soc.* **2003**, *125* (26), 7782−7783.
(106) Cao, B. P.; Wakahara, T.; Tsuchiya, T.; Kondo, M.; Maeda, Y.; Rahman, G. M. A.; Akasaka, T.; Kobayashi, K.; Nagase, S.; Yamamoto, K. *J. Am. Chem. Soc.* **2004**, *126* (30), 9164−9165.
(107) Alvarez, M. M.; Gillan, E. G.; Holczer, K.; Kaner, R. B.; Min, K. S.; Whetten, R. L. *J. Phys. Chem.* **1991**, *95* (26), 10561−10563.
(108) Akasaka, T.; Nagase, S.; Kobayashi, K.; Walchli, M.; Yamamoto, K.; Funasaka, H.; Kako, M.; Hoshino, T.; Erata, T. *Angew. Chem., Int. Ed. Engl.* **1997**, *36* (15), 1643−1645.

(109) Zhang, J.; Hao, C.; Li, S. M.; Mi, W. H.; Jin, P. *J. Phys. Chem. C* **2007**, *111* (22), 7862−7867.
(110) Keith, T. A. *AIMAll (Version 08.05.04)*; http://aim.tkgristmill.com, 2008.
(111) Kobayashi, K.; Nagase, S. *Chem. Phys. Lett.* **1999**, *302* (3−4), 312−316.

at the bond critical points.[74] In particular, Macchi and Sironi[112] have shown that covalent bonds between transition metals are characterized by (i) the small values of ρ_{bcp} and $\nabla^2\rho_{bcp}$, (ii) negative total energy density $H_{bcp} < 0$ (that is, in covalent bonds the always negative potential energy dominates over the always positive inetic energy), and (iii) the ratio of the kinetic energy density G_{bcp} to the ρ_{bcp}, which is smaller than 1. For the "closed-shell" interactions (e.g., ionic bonds, hydrogen bonds, van der Waals bonds) $H_{bcp} > 0$ and $G_{bcp}/\rho_{bcp} > 1$. H_{bcp}/ρ_{bcp} and G_{bcp}/ρ_{bcp} values for La$\cdots$La bcp in La$_2$@C$_{80}$, -0.10 and 0.37 h e^{-1}, respectively, point to the certain degree of covalency in the La$\cdots$La interactions. For comparison, Co$-$Co bond in D_{3d}-Co$_2$(CO)$_8$ is characterized by the following values: $\rho_{bcp} = 0.23$ e Å^{-3}, $\nabla^2\rho_{bcp} = 0.02$ e Å^{-5}, $H_{bcp}/\rho_{bcp} = -0.30$ h e^{-1}, and $G_{bcp}/\rho_{bcp} = 0.31$ h e^{-1}.[112] However, the strength of covalent La$\cdots$La interaction is very weak as can be shown by the small values of ρ_{bcp}, H_{bcp}, as well as La$-$La delocalization index, δ(La, La) $= 0.08$, which has the meaning of the bond order. Since La atoms carry considerable positive charges (Table 5), repulsive electrostatic interactions between two La atoms are much stronger.

In accordance with the spatial distribution of the LUMO, spin density in La$_2$@C$_{2n}$ is primarily localized on and between two La atoms (see Figure 9c for spin density distribution in La$_2$@C$_{80}^-$, and Figure S7 for La$_2$@C$_{72}^-$ and La$_2$@C$_{78}^-$). Spin populations in all three dilanthanofullerenes are 1.01 (La$_2$@C$_{72}^-$), 0.95 (La$_2$@C$_{78}^-$) and 0.96 (La$_2$@C$_{80}^-$). Localization of the spin density on La atoms is confirmed by the large a(^{139}La) hfc value reported for La$_2$@C$_{80}$ anion ($a_{iso} = 386$ G[113] and $a_{XX} = 337$ G, $a_{YY} = 333$ G, $a_{ZZ} = 423$ G[114]). SRD-PBE/Λ11 calculations predict a(^{139}La) of 592 G (the values of 617 and 523 G are also predicted for La$_2$@C$_{72}^-$ and La$_2$@C$_{78}^-$, respectively). Bader analysis of the electron density in La$_2$@C$_{2n}^-$ anions shows that even for these species the changes of La atomic charges are much smaller than expected based on the spin density distribution. In particular, La charges are decreased by only -0.21, -0.18, and -0.13 in La$_2$@C$_{72}^-$, La$_2$@C$_{78}^-$, and La$_2$@C$_{80}^-$. The spatial distribution of the $[\rho$(La$_2$@C$_{80}^-$) $- \rho$(La$_2$@C$_{80}$)] difference density clearly shows the appearance of the lobes with negative $\Delta\rho_{-/0}$ close to La atoms which have no analogues in the spin density distribution of the same cluster. Interestingly, addition of the electron to La$_2$@C$_{80}$ results in the considerable increase of the La$-$La covalent interactions. QTAIM analysis shows that La$-$La bond order (δ(La, La) delocalization index) in La$_2$@C$_{80}^-$ is increased to 0.39 (vs 0.08 in La$_2$@C$_{80}$), while bcp descriptors have the following values: $\rho_{bcp} = 0.16$ e Å^{-3}, $\nabla^2\rho_{bcp} = -0.09$ e Å^{-5}, $H_{bcp}/\rho_{bcp} = -0.24$ h e^{-1}, and $G_{bcp}/\rho_{bcp} = 0.20$ h e^{-1}.

Conclusions

In this work we reported the first detailed DFT study of the anion radical Sc$_3$N@C$_{80}^-$. First, results of our calculations clearly show that the ground state of the cluster in the anionic form, which has C_{3v} symmetry with all Sc atoms coordinated to pentagon/hexagon edges, is different from that in the neutral Sc$_3$N@C$_{80}$. In the latter, the C_3-symmetric configuration has the

lowest energy. Moreover, with the increase of the charge, the barrier to the cluster rotation with respect to the carbon cage is increased.

Earlier electrochemical studies of Sc$_3$N@C$_{80}$ indicated that the first reduction of Sc$_3$N@C$_{80}$ is quasi-reversible, indicating that follow-up chemical reaction occurs upon the electron transfer to the clusterfullerene.[12,14,21] As the reaction with the solvent is excluded by chemical reversibility of the reduction, either an intramolecular rearrangement or an intermolecular reaction between reduced species (e.g., dimerization) must be considered to explain the experimentally observed phenomena. The observation of the stable anion radical of Sc$_3$N@C$_{80}^-$ formally excludes the second alternative for this fullerene, thus limiting the possible follow-up reaction to the internal rearrangement in Sc$_3$N@C$_{80}^-$, which agrees with the results of this work. However, the current explanation still cannot be considered as definitive because (i) the increase of the cluster rotation barrier is probably not sufficient to result in an irreversibility observed at the cyclic voltammetry time scale; (ii) the anion radical Sc$_3$N@C$_{80}^-$ can be in equilibrium with the dimer (which is therefore diamagnetic), as was already reported for Sc$_3$N@C$_{68}^-$.[81] In the case of the reversible dimerization, the ESR signal still can be observed, but the electrochemical reduction may become irreversible at the low scan rates. Quantitative ESR measurements with spin counting are required to clarify this question.

DFT calculations have also shown that a(Sc) hfc in Sc$_3$N@C$_{80}^-$ is strongly dependent on the Sc position with respect to the nearest carbon atoms, the values of a(Sc) in different conformers varying by up to 40 G. We have shown that it is the direct term in a(Sc) arising from 4s contribution to the SOMO which is changing with the cluster orientation, while the polarization term, ca. -10 G, is almost constant for any cluster position. The largest value of a(Sc) is found for the lowest energy C_{3v} conformer; however, even for this conformer DFT-predicted a(Sc) is significantly underestimated by standard DFT functionals.

The study of the charge distribution in Sc$_3$N@C$_{80}^-$ revealed an interesting peculiarity which was then shown to be a general rule for all endohedral fullerenes with metal-based LUMO. While the spin density resulting from the electron transfer is primarily localized on the cluster, the charge state of the cluster is almost the same in all charge forms. This happens because the cage-to-cluster electron donation is reduced by approximately the same extent as the metal d-orbitals are occupied by the surplus electron, and hence an excess negative charge is delocalized over the carbon cage instead of being localized on the cluster. The ions with separated charge and spin sites are known in organic chemistry as "distonic ions", the term introduced by Yates, Bouma, and Radom for those radical ions that formally arise from the ionization of diradicals or zwitterions.[115,116] By their definition, spatial charge$-$spin separation in distonic ions is mandatory, i.e. it arises from the nature of the formal noncharged precursors. Recently, Tomazela et al.[117] introduced the term "distonoid ions" for those ions, in which charge$-$spin separation is not mandatory, i.e. it does not inevitably follow from the structure of the noncharged precursors. Results of this work show that endohedral fullerenes with metal-based LUMO form a special class of distonoid anions.

(112) Macchi, P.; Sironi, A. *Coord. Chem. Rev.* **2003**, *238−239*, 383–412.

(113) Dinse, K. P.; Kato, T., Multi-Frequency EPR Study of Metallo-Endofullerenes. In *Novel NMR and EPR Techniques, Lect. Notes Phys. 684*; Dolinšek, J., Vilfan, M., Žumer, S., Eds.; Springer: Berlin, Heidelberg, 2006; pp 185−207.

(114) Kato, T. *J. Mol. Struct.* **2007**, *838* (1−3), 84–88.

(115) Yates, B. F.; Bouma, W. J.; Radom, L. *J. Am. Chem. Soc.* **1984**, *106*, 5805.

(116) Yates, B. F.; Bouma, W. J.; Radom, L. *Tetrahedron* **1986**, *42*, 6225.

(117) Tomazela, D. M.; Sabino, A. A.; Sparrapan, R.; Gozzo, F. C.; Eberlin, M. N. *J. Am. Soc. Mass. Spectrom.* **2006**, *17*, 1014–1022.

Supporting Information Available: UV−vis absorption spectra of $Sc_3N@C_{80}$ and $Y_3N@C_{80}$; variation of Sc−N bond with the cluster rotation; table with $a(Sc)$ and relative energies of $Sc_3N@C_{80}^-$ anion at different values of the cluster rotation φ computed at the B3LYP//PBE level; $\Delta\rho_{neutr}$ and $\Delta\rho_{ion}$ distribution for $Sc_3N@C_{68}$ and $Sc_3N@C_{78}$ as compared to $Sc_3N@C_{80}$; $[\rho(Sc_3N@C_{80}) - \rho(C_{80}^{6-}) - \rho(Sc_3N^{6+})])$ plotted with different isodensity values; spin density distribution in anion radicals of selected endohedral fullerenes. This material is available free of charge via the Internet at http://pubs.acs.org.

JA804226A